J. Fluid Mech. (1999), *vol.* 396, *pp.* 1–36. Printed in the United Kingdom

Fully nonlinear internal waves in a two-fluid system

By WOOYOUNG CHOI AND ROBERTO CAMASSA†

Theoretical Division and Center for Nonlinear Studies,
Los Alamos National Laboratory, Los Alamos, NM 87545, USA

(Received 20 January 1999 and in revised form 12 April 1999)

Model equations that govern the evolution of internal gravity waves at the interface of two immiscible inviscid fluids are derived. These models follow from the original Euler equations under the sole assumption that the waves are long compared to the undisturbed thickness of one of the fluid layers. No smallness assumption on the wave amplitude is made. Both shallow and deep water configurations are considered, depending on whether the waves are assumed to be long with respect to the total undisturbed thickness of the fluids or long with respect to just one of the two layers, respectively. The removal of the traditional weak nonlinearity assumption is aimed at improving the agreement with the dynamics of Euler equations for large-amplitude waves. This is obtained without compromising much of the simplicity of the previously known weakly nonlinear models. Compared to these, the fully nonlinear models' most prominent feature is the presence of additional nonlinear dispersive terms, which coexist with the typical linear dispersive terms of the weakly nonlinear models. The fully nonlinear models contain the Korteweg–de Vries (KdV) equation and the Intermediate Long Wave (ILW) equation, for shallow and deep water configurations respectively, as special cases in the limit of weak nonlinearity and unidirectional wave propagation. In particular, for a solitary wave of given amplitude, the new models show that the characteristic wavelength is larger and the wave speed is smaller than their counterparts for solitary wave solutions of the weakly nonlinear equations. These features are compared and found in overall good agreement with available experimental data for solitary waves of large amplitude in two-fluid systems.

1. Introduction

Nonlinearity and dispersion are two fundamental mechanisms of gravity wave propagation in fluids. As a general rule, it is well known that nonlinearity tends to steepen a given wave form during the course of its evolution, while dispersion has the opposite effect and tends to flatten steep free-surface gradients. The case of waves at the free-surface of a homogeneous layer of incompressible and inviscid fluid offers perhaps the simplest set-up for observing the interplay between nonlinearity and dispersion. One of the most striking manifestations of these two opposing effects lies in the possibility of a balance, which results in a single wave of elevation, a solitary wave, propagating at the free surface without change in form. A commonly accepted way of quantifying the relative importance of nonlinearity and dispersion

† Present address: Department of Mathematics, University of North Carolina at Chapel Hill, Chapel Hill, NC 27599, USA.

is to introduce two independent non-dimensional parameters: the nonlinearity ratio $\alpha = a/h_1$ of wave amplitude a and fluid layer thickness h_1 and the aspect ratio $\epsilon = h_1/L$ between h_1 and a typical wavelength L. The balance responsible for creating a solitary wave is then usually taken to be a scaling relation between α and ϵ, in the form of a power law, for asymptotic values $\alpha \ll 1$ and $\epsilon \ll 1$.

The next level in complexity is offered by the case of gravity waves at the interface of two immiscible fluids of different densities. In addition to the two parameters α and $\epsilon = h_1/L$ above, where h_1 can now be taken to be the thickness of the upper fluid layer, there exists another independent parameter, the depth ratio $\gamma = h_2/h_1$, where h_2 is the thickness of the lower fluid layer. Even within the weakly nonlinear long-wave limit of $\alpha \ll 1$ and $\epsilon \ll 1$, the relative magnitude of α and ϵ for the balance between nonlinearity and dispersion can vary according to $\gamma = h_2/h_1$. Different regimes are possible depending on the depth ratio, ranging between the two extremes of lower fluid layer thickness that is also small compared to the typical wavelength, and a lower fluid layer that can be considered effectively infinite.

For shallow water characterized by $\gamma = O(1)$, the scaling $\alpha = O(\epsilon^2)$ with $\epsilon \ll 1$ leads to the Korteweg–de Vries (KdV) equation as the evolution equation governing the unidirectional propagation of weakly nonlinear long waves (Benjamin 1966). When the depth of the lower layer is much larger than that of the upper layer ($\gamma \gg 1$), the scaling $\alpha = O(\epsilon)$ leads to the Intermediate Long Wave (ILW) equation (Joseph 1977; Kubota, Ko & Dobbs 1978). It reduces to the Benjamin–Ono (BO) equation in the limit of $\gamma \to \infty$ (Benjamin 1967; Davis & Acrivos 1967; Ono 1975). More general forms of equations valid for arbitrary γ have been recently derived by Matsuno (1993) and Choi & Camassa (1996*a*) under the assumption of weak nonlinearity. The common feature of all these models is that by focusing on specific regimes and initial conditions and taking advantage of the ensuing small parameters (such as α and ϵ), the dependence on the vertical coordinate is eliminated, thereby affording a substantial simplification of the problem. However, to be useful in practice, it is necessary that the approximation to the original Euler equation be accurate even for relatively large values of the expansion parameters α and ϵ. This is in order to ensure 'robustness' against other neglected physical effects, such as viscosity. Unfortunately, there seems to be no way of ascertaining *a priori* whether a given model possesses this property. For instance, in the case of one deep fluid layer ($\gamma \gg 1$), the BO and ILW equations might very well capture the correct asymptotic behaviour of the Euler equations as α and ϵ approach zero. However, the experimental data collected by Koop & Butler (1981) provide evidence that just when these weakly nonlinear models should become good approximations to the Euler system, viscosity effects become important and compete with dispersion and nonlinearity, making these models (as well as the original Euler equations) impractical. In particular, the weak nonlinearity (small amplitude) assumption seems inadequate for most of the experimental data collected by these authors.

Despite their physical relevance, the effects of finite amplitude have received much less attention than the predominantly dispersive phenomena exhibited by weakly nonlinear models. This is perhaps due to the belief that outside certain special situations (as in e.g. stationary solutions) accurate description of finite-amplitude effects, especially dynamical ones, can ultimately be achieved only within the full Euler equations. Unfortunately, these equations are not easily amenable to analytical investigations, and their numerical integration in the presence of free surfaces is notoriously expensive, even in the simplest case of just one horizontal direction. The purpose of this paper is to show that, at least within the class of physical situations

relative to two-fluid systems, models comparable in simplicity to weakly nonlinear ones have the potential of accurately describing finite-amplitude dynamical effects.

In an effort towards a comprehensive study of two-fluid fully nonlinear internal waves, we present here a theoretical investigation of both shallow and deep water configurations. The former is the one most commonly examined in the literature. By using a numerical scheme based on Fourier cosine series of large wavelength in the stationary Euler equations, Funakoshi & Oikawa (1986) obtained steady solitary wave solutions of finite amplitude in a two-fluid system of finite depth as well as internal bore (or front) solutions joining smoothly two uniform states of constant depths at infinity. They found that, when $\gamma = O(1)$, the KdV theory is valid even for fairly moderate-amplitude waves except when the depth ratio is close to a critical value, where the coefficient of the nonlinear term in the KdV equation vanishes. In this case, Funakoshi & Oikawa show that the *modified* KdV equation, with an additional cubic nonlinear term, becomes the appropriate weakly nonlinear evolution equation. As the wave amplitude increases, the KdV equation ceases to be valid and Funakoshi & Oikawa's numerical computations show that highly nonlinear waves tend to be wider and slower than weakly nonlinear waves of the same amplitude. It is remarkable that *near criticality* the modified KdV equation continues to provide a good approximation, even for large amplitudes, at least as far as the wave profile is concerned. Computations of steady waves have been further refined for even the highest waves by Evans & Ford (1996) using a boundary integral technique for two-fluid Euler equations.

The parameters chosen in the studies mentioned above lie in the regime of shallow water, and any results for $\gamma \gg 1$ are rarely found in earlier works. Moreover, all formulations used in these studies are only valid for steady waves, i.e. no time-dependent wave evolution is addressed besides that of uniform translation. It is therefore desirable to derive a simple nonlinear model, capable of dealing with unsteady waves, whose steady solutions possess all the essential features of finite-amplitude internal waves found earlier. To the best of our knowledge, so far such a finite-amplitude reduction from two-fluid Euler equations in the spirit of weakly nonlinear models has not been attempted.

Throughout the present study, we will assume that the internal waves are long compared with at least one of the thicknesses of the fluid layers, which for definiteness we take to be that of the upper fluid. The opposite situation (thin lower layer), more pertinent to atmospheric flows, can be accounted for by a simple variable transformation. We also concentrate on the case of a fluid contained between two rigid walls at the top and bottom, with the bottom possibly removed to infinity. Thus our equations track only one (interfacial) free surface. Our techniques would work for a free top surface, but so much is gained in the simplicity of the resulting equations without compromising the essential features of our models that we feel there is no need to remove the assumption of a rigid top wall in the present study. In terms of the parameters α and ϵ introduced above, the regimes in our study satisfy $\epsilon \ll 1$ and $\alpha = O(1)$.

The paper is organized as follows. We derive model equations to describe the evolution of finite-amplitude long internal waves in §§ 3.1 and 4.1 for shallow and deep water configurations, respectively. In the shallow water case, the set of equations derived here by using a systematic asymptotic expansion method can be considered as the two-layer version of equations derived by Green & Naghdi (1976) for a homogeneous layer. For steady solutions, we show that this set of equations reduces to a nonlinear ordinary differential equation derived by Miyata (1985) by using ap-

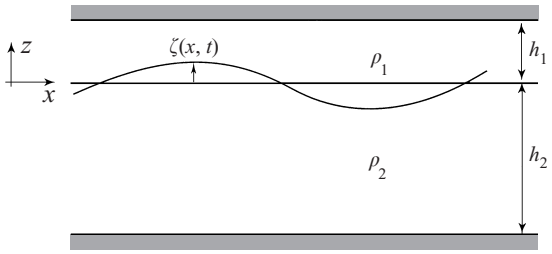

FIGURE 1. A two-fluid system

proximate conservation laws for long waves in shallow water. For the deep water configuration, our model extends the one introduced by Choi & Camassa (1996*b*) for an *infinitely* deep water configuration. The models we derive conserve all the basic physical quantities such as mass, momentum and energy, and possess a variational formulation. In §§ 3.3 and 4.3, several properties of solitary wave solutions are discussed and compared with weakly nonlinear solutions given in §§ 3.2 and 4.2. The finite-amplitude model shows that no solitary wave solution can be found beyond a certain amplitude at which only a front solution exists. This front solution is compared with the exact solutions of the Euler equations in § 3.4. We find that all the features of steady solitary wave solutions of the new models are consistent with those determined by earlier numerical solutions of the Euler equations. Moreover, we examine in detail the scaling law between wave amplitude and characteristic wavelength with the aim of comparing the model with the experiment by Koop & Butler (1981). We remark that the new models support bidirectional wave propagation, and their extension to two (horizontal) spatial dimensions is straightforward. In the Appendix, we propose several alternative ways to further simplify these models, for both shallow and deep water configurations, in the case of unidirectional wave propagation, while retaining some extra nonlinearity with respect to the weakly nonlinear (KdV and ILW) models.

2. Governing equations

For an inviscid and incompressible fluid of density ρ_i, the velocity components in Cartesian coordinates (u_i, w_i) and the pressure p_i satisfy the continuity equation and the Euler equations,

$$u_{ix} + w_{iz} = 0, \tag{2.1}$$

$$u_{it} + u_i u_{ix} + w_i u_{iz} = -p_{ix}/\rho_i, \tag{2.2}$$

$$w_{it} + u_i w_{ix} + w_i w_{iz} = -p_{iz}/\rho_i - g, \tag{2.3}$$

where g is the gravitational acceleration and subscripts with respect to space and time represent partial differentiation. In a two-fluid system, $i = 1$ ($i = 2$) stands for the upper (lower) fluid (see figure 1) and $\rho_1 < \rho_2$ is assumed for a stable stratification.

The boundary conditions at the interface are the continuity of normal velocity and pressure:

$$\zeta_t + u_1\zeta_x = w_1, \quad \zeta_t + u_2\zeta_x = w_2, \quad p_1 = p_2 \quad \text{at} \quad z = \zeta(x,t), \tag{2.4}$$

where ζ is a displacement of the interface. At the upper and lower rigid surfaces, the kinematic boundary conditions are given by

$$w_1(x, h_1, t) = 0, \qquad w_2(x, -h_2, t) = 0, \tag{2.5}$$

where h_1 (h_2) is the undisturbed thickness of the upper (lower) fluid layer.

From the linearized problem of (2.1)–(2.5), the dispersion relation between wave speed c and wavenumber k (Lamb 1932, § 231) is

$$c^2 = \frac{(g/k)(\rho_2 - \rho_1)}{\rho_1 \coth kh_1 + \rho_2 \coth kh_2}. \tag{2.6}$$

Under the long-wave assumption ($kh_1 \to 0$), the asymptotic behaviour of the linear dispersion relation varies depending on the depth ratio or, equivalently, kh_2: as $kh_i \to 0$ (shallow water),

$$c = c_0 \left[1 - \frac{k^2}{6} \frac{\rho_1 h_1^2 h_2 + \rho_2 h_1 h_2^2}{\rho_1 h_2 + \rho_2 h_1} + O(k^4 h_i^4)\right], \quad c_0^2 = \frac{g h_1 h_2 (\rho_2 - \rho_1)}{\rho_1 h_2 + \rho_2 h_1}; \tag{2.7}$$

as $kh_1 \to 0$ and $kh_2 = O(1)$ (deep water),

$$c = c_0 \left[1 - \frac{1}{2}\left(\frac{\rho_2}{\rho_1}\right) kh_1 \coth kh_2 + O(k^2 h_1^2)\right], \quad c_0^2 = g h_1 \left(\frac{\rho_2}{\rho_1} - 1\right); \tag{2.8}$$

and, as $kh_1 \to 0$ and $kh_2 \to \infty$ (infinitely deep water),

$$c = c_0 \left[1 - \frac{1}{2}\left(\frac{\rho_2}{\rho_1}\right) |k| h_1 + O(k^2 h_1^2)\right], \quad c_0^2 = g h_1 \left(\frac{\rho_2}{\rho_1} - 1\right). \tag{2.9}$$

These different linear dispersion relations result in different linear dispersive terms in weakly nonlinear models such as the KdV, ILW and BO equations for shallow, deep and infinitely deep water configurations, respectively.

3. Shallow water configuration

3.1. *Fully nonlinear model*

From the assumption that the thickness of each fluid layer is much smaller than the characteristic wavelength, the continuity equation (2.1) yields the following scaling relation between u_i and w_i:

$$w_i/u_i = O(h_i/L) = O(\epsilon) \ll 1, \tag{3.1}$$

where L is a typical wavelength. For finite-amplitude waves, we also assume that

$$u_i/U_0 = O(\zeta/h_i) = O(1), \tag{3.2}$$

where U_0 is a characteristic speed chosen as $U_0 = (g h_1)^{1/2}$. Based on the scalings in (3.1)–(3.2), we non-dimensionalize all physical variables as

$$\left.\begin{aligned} x = L x^*, \quad z = h_1 z^*, \quad t = (L/U_0) t^*, \\ \zeta = h_1 \zeta^*, \quad p_i = (\rho_1 U_0^2) p_i^*, \quad u_i = U_0 u_i^*, \quad w_i = \epsilon U_0 w_i^*, \end{aligned}\right\} \tag{3.3}$$

and assume that all variables adorned with asterisks are $O(1)$ in ϵ.

We focus on the upper fluid first; the analysis for the lower fluid follows along similar lines. By integrating (2.1)–(2.2) for $i = 1$ across the upper-fluid layer ($\zeta \leqslant z \leqslant 1$) and imposing the boundary conditions (2.4)–(2.5), we obtain the layer-mean equations for the upper fluid (see e.g. Wu 1981 or Camassa & Levermore 1997),

$$\eta_{1t} + (\eta_1 \overline{u}_1)_x = 0, \qquad \eta_1 = 1 - \zeta, \tag{3.4}$$

$$(\eta_1 \overline{u}_1)_t + (\eta_1 \overline{u_1 u_1})_x = -\eta_1 \overline{p_{1x}}, \tag{3.5}$$

where the layer-mean quantity $\bar{f}$ of any function $f(x,z,t)$ is defined as

$$\bar{f}(x,t) = \frac{1}{\eta_1}\int_{\zeta}^{1} f(x,z,t)\mathrm{d}z. \tag{3.6}$$

and we have dropped the asterisks for dimensionless variables. The quantities $\overline{u_1 u_1}$ and $\overline{p_{1x}}$ prevent closure of the system of layer-mean equations (3.4)–(3.5). The following analysis will therefore focus on expressing these quantities in terms of the two unknowns ζ and $\bar{u}_1$.

From (3.3), the vertical momentum equation (2.3) for the upper fluid can be written as

$$p_{1z} = -1 - \epsilon^2[w_{1t} + u_1 w_{1x} + w_1 w_{1z}]. \tag{3.7}$$

Hence, we can seek an asymptotic expansion of $f = (u_1, w_1, p_1)$ in powers of ϵ^2,

$$f(x,z,t) = f^{(0)} + \epsilon^2 f^{(1)} + O(\epsilon^4), \tag{3.8}$$

where $f^{(m)} = O(1)$ for $m = 0, 1, \ldots$.

From (3.7)–(3.8) and by imposing the pressure continuity across the interface given by (2.4), the leading-order pressure $p_1^{(0)}$ is

$$p_1^{(0)} = -(z - \zeta) + P(x,t), \tag{3.9}$$

where $P(x,t) = p_2(x,\zeta,t)$ is the pressure at the interface. By substituting (3.8)–(3.9) into (2.2), one obtains

$$u_1^{(0)} = u_1^{(0)}(x,t) \quad \text{if } u_{1z}^{(0)} = 0 \quad \text{at } t = 0. \tag{3.10}$$

Notice that condition (3.10) is automatically satisfied if we assume that the flow is initially irrotational (Choi & Camassa 1996*a*). From (2.1) for $i = 1$, we can now obtain the leading-order vertical velocity $w_1^{(0)}$ that satisfies the kinematic boundary condition (2.4) at the interface:

$$w_1^{(0)} = -(u_{1x}^{(0)})(z - \zeta) + \mathrm{D}_1\zeta, \tag{3.11}$$

where D_i stands for the material derivative,

$$\mathrm{D}_i = \partial_t + u_i^{(0)}\partial_x. \tag{3.12}$$

From (3.8) and (3.10), it is easy to show that

$$\eta_1\overline{u_1 u_1} = \eta_1 \bar{u}_1\,\bar{u}_1 + O(\epsilon^4), \tag{3.13}$$

so that the layer-mean horizontal momentum equation (3.5) in dimensionless form becomes

$$\bar{u}_{1t} + \bar{u}_1\bar{u}_{1x} = -\overline{p_{1x}} + O(\epsilon^4). \tag{3.14}$$

At $O(\epsilon^2)$, from (3.7)–(3.8) and (3.11), the equation for $p_1^{(1)}$ is

$$\begin{aligned} p_{1z}^{(1)} &= -\left[w_{1t}^{(0)} + u_1^{(0)}w_{1x}^{(0)} + w_1^{(0)}w_{1z}^{(0)}\right] \\ &= G_1(x,t)(z - \zeta) - \eta_1 G_1(x,t). \end{aligned} \tag{3.15}$$

In this equation for $p_1^{(1)}$, G_1 denotes

$$G_1(x,t) = \bar{u}_{1xt} + \bar{u}_1\bar{u}_{1xx} - (\bar{u}_{1x})^2 = \frac{(\mathrm{D}_1^2\zeta)}{\eta_1} + O(\epsilon^2), \tag{3.16}$$

where we have used (3.4) and $\overline{u}_1 = u_1^{(0)} + O(\epsilon^2)$ for the last equality. After integrating (3.15) with respect to z and imposing the dynamic boundary condition in (2.4), we obtain $p_1^{(1)}$:

$$p_1^{(1)}(x,z,t) = \tfrac{1}{2}G_1(x,t)(z-\zeta)^2 - \eta_1 G_1(x,t)(z-\zeta). \tag{3.17}$$

From (3.9) and (3.17), the right-hand-side term of the horizontal momentum equation (3.14) is therefore

$$\overline{p_{1x}} = \overline{\left(p_{1x}^{(0)} + \epsilon^2 p_{1x}^{(1)}\right)} + O(\epsilon^4) = \zeta_x + P_x - \frac{\epsilon^2}{\eta_1}\left(\tfrac{1}{3}\eta_1^3 G_1\right)_x + O(\epsilon^4). \tag{3.18}$$

After substituting (3.18) for $\overline{p_{1x}}$, (3.4) and (3.14) provide the desired set of equations governing the motion of the upper fluid.

Rather than repeating the same procedure for the lower fluid layer, we simply notice that, by replacing (ζ, g) by $(-\zeta, -g)$ and the subscript 1 by 2, we can obtain a set of equations for the lower fluid directly from (3.4) and (3.14). The final result for the complete set of equations for the four unknowns $(\zeta, \overline{u}_1, \overline{u}_2, P)$ is, in dimensional form,

$$\eta_{1t} + (\eta_1 \overline{u}_1)_x = 0, \qquad \eta_1 = h_1 - \zeta, \tag{3.19}$$

$$\eta_{2t} + (\eta_2 \overline{u}_2)_x = 0, \qquad \eta_2 = h_2 + \zeta, \tag{3.20}$$

$$\overline{u}_{1t} + \overline{u}_1\overline{u}_{1x} + g\zeta_x = -\frac{P_x}{\rho_1} + \frac{1}{\eta_1}\left(\tfrac{1}{3}\eta_1^3 G_1\right)_x + O(\epsilon^4), \tag{3.21}$$

$$\overline{u}_{2t} + \overline{u}_2\overline{u}_{2x} + g\zeta_x = -\frac{P_x}{\rho_2} + \frac{1}{\eta_2}\left(\tfrac{1}{3}\eta_2^3 G_2\right)_x + O(\epsilon^4), \tag{3.22}$$

with G_1 given by (3.16) and

$$\overline{u}_2(x,t) = \frac{1}{\eta_2}\int_{-h_2}^{\zeta} u_2(x,z,t)\,\mathrm{d}z, \quad G_2(x,t) = \overline{u}_{2xt} + \overline{u}_2\overline{u}_{2xx} - (\overline{u}_{2x})^2 = -\frac{(\mathrm{D}_2^2\zeta)}{\eta_2}. \tag{3.23}$$

Notice that the two kinematic equations, (3.19) and (3.20), are exact while the dynamic equations, (3.21) and (3.22), have an error of $O(\epsilon^4)$.

The fact that internal waves in this system have 'two degrees of freedom' (left- and right-going waves) suggests that (3.19)–(3.22) should reduce to a second-order system of two evolution equations. By eliminating ζ from (3.19)–(3.20) and imposing zero boundary conditions at infinity, $\overline{u}_2$ can be expressed in terms of $\overline{u}_1$ as

$$\overline{u}_2 = -\left(\frac{\eta_1}{\eta_2}\right)\overline{u}_1. \tag{3.24}$$

After substituting (3.22) into (3.21) for P_x and using (3.24) for $\overline{u}_2$, (3.19) and (3.21) become a closed system of equations for ζ and $\overline{u}_1$.

If the upper fluid layer is neglected and P is regarded as the external pressure applied to the free surface, (3.20) and (3.22) are the complete set of evolution equations for a homogeneous layer, originally derived by Green & Naghdi (1976) by using the so-called 'director-sheet' theory. Therefore (3.19)–(3.22) can be regarded as the (coupled) Green–Naghdi (GN) equations for one-dimensional internal waves in a two-fluid system. This set of equations can also be obtained as in Liska, Margolin & Wendroff (1995) by assuming *a priori* that w_i is a linear function of z directly in the governing equations of § 2.

The system (3.19)–(3.22) has the following four conserved quantities:

$$\frac{\mathrm{d}\mathscr{M}}{\mathrm{d}t} \equiv \frac{\mathrm{d}}{\mathrm{d}t}\int \zeta \,\mathrm{d}x = 0, \tag{3.25}$$

$$\frac{\mathrm{d}\mathscr{I}}{\mathrm{d}t} \equiv \frac{\mathrm{d}}{\mathrm{d}t}\int \left(\overline{u}_i + \tfrac{1}{6}\eta_i^2 \overline{u}_{ixx}\right) \mathrm{d}x = 0 \qquad (i = 1, 2), \tag{3.26}$$

$$\frac{\mathrm{d}\mathscr{P}}{\mathrm{d}t} \equiv \frac{\mathrm{d}}{\mathrm{d}t}\int (\rho_1\eta_2\overline{u}_1 + \rho_2\eta_1\overline{u}_2)\,\mathrm{d}x = 0, \tag{3.27}$$

$$\frac{\mathrm{d}\mathscr{E}}{\mathrm{d}t} \equiv \frac{\mathrm{d}}{\mathrm{d}t}\left[\int \tfrac{1}{2}(\rho_2 - \rho_1)g\zeta^2\,\mathrm{d}x + \sum_{i=1}^{2}\int \tfrac{1}{2}\rho_i\left(\eta_i\overline{u}_i^2 + \tfrac{1}{3}\eta_i^3\overline{u}_{ix}^2\right)\mathrm{d}x\right] = 0, \tag{3.28}$$

which correspond to conservation laws for mass, irrotationality, horizontal momentum, and energy. In fact, the second conservation law (3.26) is related to the 'trivial' conservation law,

$$\frac{\mathrm{d}}{\mathrm{d}t}\int u_i\,\mathrm{d}x = 0, \tag{3.29}$$

which, after imposing the condition that the flow has zero horizontal component of vorticity $w_{ix} = u_{iz}$ (i.e. the flow is irrotational in the two-dimensional set-up of this paper), follows easily from the horizontal momentum equation of the Euler system (2.2) (see Camassa & Levermore 1997 for more details on this point). We also remark that the energy conservation law (3.28) can be placed within a Hamiltonian structure that generalizes that of a single-layer Green–Naghdi model (cf. Camassa, Holm & Levermore 1996).

One final remark on the structure of the coupled GN system is in order. As pointed out by Liska *et al.* (1995), the dispersion relation obtained from (3.19)–(3.22) by linearizing around a state in which one of the two fluids moves with constant velocity with respect to the other (always assumed to be at rest by Galileian invariance) is ill posed, i.e. unstable to all sufficiently large-wavenumber modes. This reflects the behaviour of the original Euler equation under the same circumstances (i.e. in the absence of surface tension between the two fluids, see e.g. Whitham 1974, p. 445). For the finite-amplitude wave motion modelled by (3.19)–(3.22), this ill-posedness could result in an instability mechanism for the waves in certain regions of the interface (see e.g. the internal bore solutions discussed in §§ 3.3 and 3.4). While the implications of this fact deserve further study, it is remarkable that the model, though outside its asymptotic range of validity, still manages to capture the legacy of a basic feature of the original Euler equations.

Next, by assuming weak nonlinearity and unidirectional wave propagation, we show that system (3.19)–(3.22) includes all the known weakly nonlinear evolution equations.

3.2. *Weakly nonlinear models*

For weakly nonlinear waves, we replace the scaling (3.2) by

$$u_i/U_0 = O(\zeta/h_i) = O(\alpha) = O(\epsilon^2). \tag{3.30}$$

Under this assumption, equations (3.19)–(3.22) become the Boussinesq equations for internal waves in a two-fluid system, because the nonlinear dispersive terms of $O(\epsilon^2)$

in the right-hand sides of (3.21)–(3.22) reduce to

$$\frac{1}{\eta_i}\left(\tfrac{1}{3}\eta_i^3 G_i\right)_x \to \tfrac{1}{3}h_i^2\bar{u}_{ixxt}. \tag{3.31}$$

Furthermore, from (3.24), we have

$$\bar{u}_2 = -\frac{h_1-\zeta}{h_2+\zeta}\,\bar{u}_1 = \left[-\frac{h_1}{h_2} + \frac{h_1+h_2}{h_2}\left(\frac{\zeta}{h_2}\right) + O(\alpha^2)\right]\bar{u}_1, \tag{3.32}$$

and, by eliminating P from (3.21) and (3.22) and using (3.32) for $\bar{u}_2$, a set of equations for ζ and $\bar{u}_1$ is obtained:

$$\zeta_t - [(h_1-\zeta)\bar{u}_1]_x = 0, \tag{3.33}$$

$$\bar{u}_{1t} + b_1\bar{u}_1\bar{u}_{1x} + (b_2+b_3\zeta)\,\zeta_x = b_4\bar{u}_{1xxt} + O(\alpha\epsilon^4, \alpha^2\epsilon^2), \tag{3.34}$$

where the b_i are given by

$$b_1 = \frac{\rho_1 h_2^2 - \rho_2 h_1 h_2 - 2\rho_2 h_1^2}{\rho_1 h_2^2 + \rho_2 h_1 h_2}, \qquad b_2 = \frac{g h_2(\rho_1-\rho_2)}{\rho_1 h_2 + \rho_2 h_1}, \tag{3.35}$$

$$b_3 = \frac{g\rho_2(\rho_1-\rho_2)(h_1^2+h_1h_2)}{(\rho_1 h_2+\rho_2 h_1)^2}, \qquad b_4 = \frac{1}{3}\frac{\rho_1 h_1^2 h_2 + \rho_2 h_1 h_2^2}{\rho_1 h_2 + \rho_2 h_1}. \tag{3.36}$$

Notice that compared with the classical Boussinesq equations for the case of a homogeneous layer (see Whitham 1974, p. 465), the second equation (3.34) contains the extra quadratic term $\zeta\zeta_x$.

For unidirectional waves, (3.33)–(3.34) can be further simplified, resulting in the KdV equation for ζ,

$$\zeta_t + c_0\zeta_x + c_1\zeta\zeta_x + c_2\zeta_{xxx} = 0, \tag{3.37}$$

where

$$c_0^2 = \frac{g h_1 h_2(\rho_2-\rho_1)}{\rho_1 h_2 + \rho_2 h_1}, \quad c_1 = -\frac{3c_0}{2}\frac{\rho_1 h_2^2 - \rho_2 h_1^2}{\rho_1 h_1 h_2^2 + \rho_2 h_1^2 h_2}, \quad c_2 = \frac{c_0}{6}\frac{\rho_1 h_1^2 h_2 + \rho_2 h_1 h_2^2}{\rho_1 h_2 + \rho_2 h_1}. \tag{3.38}$$

The solitary wave solution is given by

$$\zeta_{KdV}(X) = a\,\mathrm{sech}^2(X/\lambda_{KdV}), \qquad X = x - ct, \tag{3.39}$$

with

$$(\lambda_{KdV})^2 = \frac{12c_2}{ac_1}, \quad c = c_0 + \frac{c_1}{3}a. \tag{3.40}$$

Notice that the coefficient c_1 of the nonlinear term in (3.38) vanishes at the critical depth ratio

$$\left(h_1/h_2\right)_c = (\rho_1/\rho_2)^{1/2}, \tag{3.41}$$

signalling that near this depth ratio nonlinear effects enter the dynamics of internal long waves at higher order in the (small) amplitude parameter α. In fact, when the depth ratio is close to the critical value (3.41), an appropriate weakly nonlinear model is provided by the modified KdV equation, where the nonlinear term is cubic in the interface variable ζ (see e.g. Funakoshi & Oikawa 1986, and the Appendix). Also notice that if h_1/h_2 is greater or smaller than the critical value, the polarity of solitary waves is positive or negative, respectively.

For small-amplitude waves, the linear dispersion relation for the bidirectional model (3.33)–(3.34) is

$$c^2 = \frac{-b_2 h_1}{1 + b_4 k^2}, \tag{3.42}$$

which reduces, for small kh_1, to that for the KdV equation (2.7).

3.3. *Travelling wave solutions*

To look for waves of permanent form travelling from left to right with constant speed c, we make the ansatz

$$\zeta(x,t) = \zeta(X), \quad \overline{u}_i(x,t) = \overline{u}_i(X), \qquad X = x - ct\,. \tag{3.43}$$

Putting this into (3.19)–(3.20) and integrating once with respect to X gives

$$\overline{u}_i = c\left(1 - \frac{h_i}{\eta_i}\right), \tag{3.44}$$

where we have assumed the asymptotic behaviour $\eta_i \to h_i$ as $|X| \to \infty$. By eliminating P from (3.21)–(3.22) and using (3.43), we have

$$\begin{aligned} K[\zeta]\zeta_X &\equiv \rho_1(-c + \overline{u}_1)\overline{u}_{1X} - \rho_2(-c + \overline{u}_2)\overline{u}_{2X} - g(\rho_2 - \rho_1)\zeta_X \\ &= \frac{\rho_1}{\eta_1}\left(\tfrac{1}{3}\eta_1^3 G_1\right)_X - \frac{\rho_2}{\eta_2}\left(\tfrac{1}{3}\eta_2^3 G_2\right)_X. \end{aligned} \tag{3.45}$$

Substituting (3.44) for $\overline{u}_i$ into (3.45) yields $K[\zeta]$ and G_i in terms of η_i, $i = 1, 2$, respectively:

$$K[\zeta] = \frac{\rho_1 c^2 h_1^2}{\eta_1^3} + \frac{\rho_2 c^2 h_2^2}{\eta_2^3} - g(\rho_2 - \rho_1), \tag{3.46}$$

and

$$G_i = -\frac{c^2 h_i^2}{\eta_i^2}\left(\frac{\eta_{iX}}{\eta_i}\right)_X. \tag{3.47}$$

Integrating (3.45) once with respect to X yields, after imposing $\eta_{iX}, \eta_{iXX} \to 0$ as $X \to -\infty$,

$$-\tfrac{1}{3}\rho_1 c^2 h_1^2\left(\frac{\eta_{1XX}}{\eta_1} - \frac{1}{2}\frac{{\eta_{1X}}^2}{\eta_1^2}\right) + \tfrac{1}{3}\rho_2 c^2 h_2^2\left(\frac{\eta_{2XX}}{\eta_2} - \frac{1}{2}\frac{{\eta_{2X}}^2}{\eta_2^2}\right) = \int_0^\zeta K[\zeta]\,\mathrm{d}\zeta, \tag{3.48}$$

where we have used $\mathrm{d}\zeta = \zeta_X \mathrm{d}X$.

We can also integrate the same equation (3.45), after multiplying by η_1, to obtain

$$\begin{aligned} -\tfrac{1}{3}\rho_1 c^2 h_1^2\left(\eta_{1XX} - \frac{{\eta_{1X}}^2}{\eta_1}\right) - \tfrac{1}{3}\rho_2 c^2 h_2^2\left(\eta_{2XX} - \frac{{\eta_{2X}}^2}{\eta_2}\right) \\ + \tfrac{1}{3}\rho_2 c^2 h_2^2(h_1 + h_2)\left(\frac{\eta_{2XX}}{\eta_2} - \frac{1}{2}\frac{{\eta_{2X}}^2}{\eta_2^2}\right) = \int_0^\zeta \eta_1 K[\zeta]\,\mathrm{d}\zeta, \end{aligned} \tag{3.49}$$

where we have used $\eta_1 = (h_1 + h_2) - \eta_2$. The fact that there exist two different ways of integrating (3.45) leading to (3.48)–(3.49) is a reflection of the existence of the two conservation laws (3.26) and (3.27). (The mass conservation law (3.25) allows the first integration leading to (3.44).) Notice that energy conservation (3.28) for travelling waves holds under (3.26) (which is related to the Bernoulli equation, see § 3.4).

After eliminating ζ_{XX} from (3.48)–(3.49) by multiplying (3.48) by η_1 and subtracting

from (3.49), we obtain the following nonlinear ordinary differential equation for ζ:

$$(\zeta_X)^2 = \frac{3\zeta^2[\rho_1 c^2\eta_2 + \rho_2 c^2\eta_1 - g(\rho_2-\rho_1)\eta_1\eta_2]}{\rho_1 c^2 h_1^2\eta_2 + \rho_2 c^2 h_2^2\eta_1}, \tag{3.50}$$

which can be rewritten as

$$(\zeta_X)^2 = \left[\frac{3g(\rho_2-\rho_1)}{c^2\left(\rho_1 h_1^2 - \rho_2 h_2^2\right)}\right]\frac{\zeta^2(\zeta-a_-)(\zeta-a_+)}{(\zeta-a_*)}. \tag{3.51}$$

In (3.51), a_* is given by

$$a_* = -\frac{h_1 h_2(\rho_1 h_1 + \rho_2 h_2)}{\rho_1 h_1^2 - \rho_2 h_2^2}, \tag{3.52}$$

and $a_\pm$ are the two roots of a quadratic equation,

$$\zeta^2 + q_1\zeta + q_2 = 0, \tag{3.53}$$

with q_1 and q_2 defined by

$$q_1 = -\frac{c^2}{g} - h_1 + h_2, \qquad q_2 = h_1 h_2\left(\frac{c^2}{c_0^2} - 1\right). \tag{3.54}$$

In this expression, c_0 is the linear long-wave speed given by (3.38).

We remark that the same equation (3.50) has been derived by Miyata (1985) by using conservation laws for steady solitary waves in shallow water. Therefore Miyata's theory is a steady version of our coupled GN equations (3.19)–(3.22).

For smooth solitary wave solutions to exist, the right-hand side of (3.51) has to be bounded and non-negative for ζ between $\zeta = 0$ and one of the two real roots of (3.53). The boundedness is ensured by the fact that a_* is always less than $-h_2$ or larger than h_1, as follows easily from expression (3.52), so that the denominator of (3.51) can never vanish within the physical range of ζ. To study the sign of the right-hand side of (3.51), it is necessary to distinguish between $\rho_1 h_1^2 - \rho_2 h_2^2 > 0$ (for which the ratio h_1/h_2 is above critical), and $\rho_1 h_1^2 - \rho_2 h_2^2 < 0$ (h_1/h_2 below critical). (Recall that it is always $\rho_2 - \rho_1 > 0$ for stable stratification.)

If $\rho_1 h_1^2 - \rho_2 h_2^2 > 0$, i.e. $h_1/h_2 > (\rho_2/\rho_1)^{1/2}$, then $a_* < -h_2$ and the product $(\zeta - a_-)(\zeta - a_+)$ must be non-negative, i.e. $\zeta < a_-$ or $\zeta > a_+$. Since the origin $\zeta = 0$ must belong to the range of admissible ζ, it follows that the two real roots $a_\pm$ of (3.53),

$$a_\pm = -\tfrac{1}{2}q_1 \pm \left(\tfrac{1}{4}q_1^2 - q_2\right)^{1/2}, \tag{3.55}$$

must have the same sign. This occurs only for q_2 positive, which, from (3.54), implies that the wave speed c must be supercritical, or

$$c^2 > c_0^2. \tag{3.56}$$

According to whether $a_- > 0$ or $a_+ < 0$, the solitary wave will be a wave of elevation or depression, respectively. It is easy to see that with $\rho_1 h_1^2 - \rho_2 h_2^2 > 0$, the supercritical speed constraint (3.56) implies $q_1 < 0$ and $a_- > 0$, so that in this case the solitary wave is one of elevation.

The opposite case $\rho_1 h_1^2 - \rho_2 h_2^2 < 0$ can be treated similarly. Under this condition, both the factor in square brackets and the denominator in (3.51) are negative (since $a_* > h_1 > 0$), and solitary waves of both polarities are possible. To summarize, we have the following three possibilities for solitary waves in the shallow water configuration:

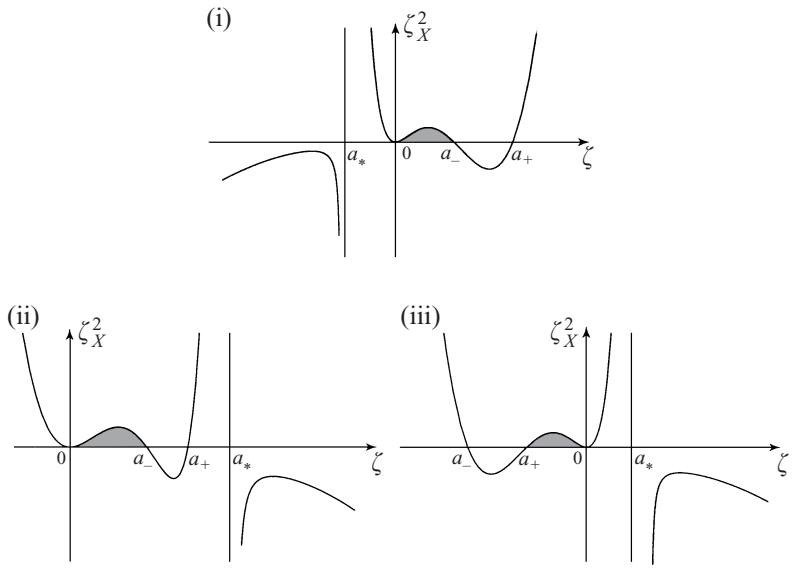

FIGURE 2. The right-hand side of (3.51) shows that solitary wave solutions exist only in shaded areas. (i) $(h_1/h_2) > (\rho_2/\rho_1)^{1/2}$ $(a_* < 0 \leqslant \zeta \leqslant a_- < a_+)$, (ii) $(\rho_1/\rho_2)^{1/2} < (h_1/h_2) < (\rho_2/\rho_1)^{1/2}$ $(0 \leqslant \zeta \leqslant a_- < a_+ < a_*)$, or (iii) $(h_1/h_2) < (\rho_1/\rho_2)^{1/2}$ $(a_- < a_+ \leqslant \zeta \leqslant 0 < a_*)$.

Case (i): $h_1/h_2 > (\rho_2/\rho_1)^{1/2}$. Then $q_1 < 0 \Rightarrow a_- > 0$, the solitary wave is of elevation.

Case (ii): $(\rho_1/\rho_2)^{1/2} < h_1/h_2 < (\rho_2/\rho_1)^{1/2}$. Then $q_1 < 0 \Rightarrow a_- > 0$ for a wave of elevation.

Case (iii): $h_1/h_2 < (\rho_1/\rho_2)^{1/2}$. Then $q_1 > 0 \Rightarrow a_+ < 0$ and the wave is of depression.

These conclusions for the existence of a solitary wave and its polarity are illustrated in figure 2.

Notice that the fully nonlinear theory once again leads to $\zeta = 0$, i.e. non-existence of solitary waves, as the solution for the critical depth ratio $h_1/h_2 = (\rho_1/\rho_2)^{1/2}$. Of the other limiting cases, when the inequalities above are replaced by equalities, the only interesting one occurs when the two roots $a_\pm$ coincide (at $q_2 = q_1^2/4$). In this case the travelling wave equation (3.51) admits a heteroclinic, rather than a homoclinic, solution which connects the fixed points $\zeta = 0$ to $\zeta = -q_1/2$. As $a_- \to a_+$, the solitary wave solution becomes broader and broader, while its amplitude tends to the limit $\zeta = -q_1/2 \equiv a_m$, which is reached just when the solitary wave degenerates into a front-like solution. We will come back to this interesting limit at the end of the section.

The phase-space analysis of equation (3.51) succeeds in giving all the qualitative information and classification for the solitary wave solutions supported by the coupled GN system (3.19)–(3.22). Of course, quantitative information can also be obtained by (3.53) (or (3.55)) and by quadratures of (3.51). In the following, whenever applicable, we will include in our examples the density ratio $\rho_1/\rho_2 = 0.63$ and depth ratio $h_1/h_2 = 5.09$, used by Koop & Butler (1981) in their shallow water configuration experiments.

We first look at wave speed vs. wave amplitude. Equation (3.53) shows that the c can be written in terms of a as

$$\frac{c^2}{c_0^2} = \frac{(h_1 - a)(h_2 + a)}{h_1 h_2 - (c_0^2/g)\, a}. \tag{3.57}$$

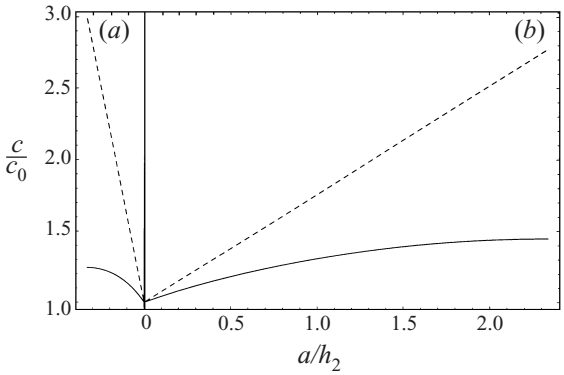

FIGURE 3. Wave speed c versus wave amplitude a for $\rho_1/\rho_2 = 0.63$: ——, fully nonlinear theory given by (3.57); – – –, weakly nonlinear (KdV) theory given by (3.40). (*a*) $h_1/h_2 = 0.2$, (*b*) $h_1/h_2 = 5$.

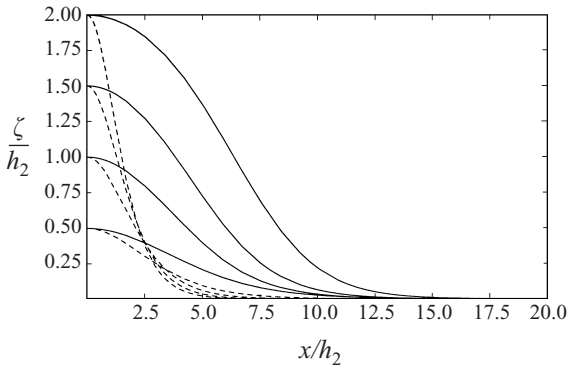

FIGURE 4. Solitary wave solutions (——) of (3.51) for $\rho_1/\rho_2 = 0.63$, $h_1/h_2 = 5.09$ and $a/h_2 =$(0.5, 1, 1.5, 2) compared with KdV solitary waves (– – –) of the same amplitude given by (3.39). Here and in the following figure of wave profiles, the waves are symmetric with respect to reflections $X \to -X$ and only half of the wave profile is shown.

As figure 3 shows, for $\rho_1/\rho_2 = 0.63$ and $h_1/h_2 = 0.2$ and 5, the solitary wave speed given by (3.57) increases with wave amplitude at a rate much slower than that of the weakly nonlinear theory given by (3.40).

Integration of (3.51) can be carried out, resulting in a wave form $\zeta(X)$ expressed implicitly by a relation $X = X_s(\zeta)$. The function X_s is a combination of elliptic integrals, and as such is not particularly informative. However, explicit knowledge of X_s does allow wave profiles to be readily obtained by plotting routines. We only report here the result pertaining to Koop & Butler's configuration, i.e. $\rho_1 h_1^2 - \rho_2 h_2^2 > 0$, whereby

$$\kappa X = \frac{2}{(a_+ - a_*)^{1/2}} \left[\left(\frac{a_+ - a_*}{a_+} \right) F(\varphi, m_1) - \frac{a_*(a_+ - a_-)}{a_+ a_-} \Pi(\varphi, \mu_1, m_1) \right]. \tag{3.58}$$

Here

$$\sin\varphi \equiv \left[\frac{(a_+ - a_*)(a_- - \zeta)}{(a_- - a_*)(a_+ - \zeta)} \right]^{1/2}, \qquad m_1^2 \equiv \frac{a_- - a_*}{a_+ - a_*}, \qquad \mu_1 \equiv \frac{a_+}{a_-} m_1^2, \tag{3.59}$$

the coefficient κ is

$$\kappa = \left| \frac{3g(\rho_2 - \rho_1)}{c^2(\rho_1 h_1^2 - \rho_2 h_2^2)} \right|^{1/2}, \tag{3.60}$$

and F and Π stand for elliptic integrals of first and third kind, respectively (Byrd & Friedman 1954). Notice that the third-kind elliptic integral Π, through its logarithmic divergence in the limit $\zeta \to 0$, is responsible for the exponential decay of the solitary waves as $|X| \to \infty$. Several plots of the solution for different amplitudes are presented in figure 4, where they are compared with the corresponding amplitude KdV solutions (3.39). As one can see from the figure, finite-amplitude solitary waves tend to be considerably wider than their weakly nonlinear counterparts.

The solitary waves generated in the experiments by Koop & Butler (1981) exhibited a similar trend between wave amplitude and wavelength. To quantify this trend, Koop & Butler introduced an integral measure of the effective wavelength, λ_I, which they defined as

$$\lambda_I \equiv \left| \frac{1}{a} \int_0^\infty \zeta(X)\, \mathrm{d}X \right| = \left| \frac{1}{a} \int_0^a \frac{\zeta(X)}{(\mathrm{d}\zeta/\mathrm{d}X)}\, \mathrm{d}\zeta \right|. \tag{3.61}$$

By substituting (3.51) for ζ_X into (3.61), we can compute λ_I for the solitary wave of the GN model in terms of elliptic integrals (Byrd & Friedman 1954). The result, for all the combinations of density and depth ratios in cases (i)–(iii), is, respectively,

$$\lambda_I = \frac{2}{\kappa a_-} \left[(a_+ - a_*)^{1/2} \left(F(\delta_1, m_1) - E(\delta_1, m_1) \right) + \left(\frac{a_- |a_*|}{a_+} \right)^{1/2} \right], \quad \text{for} \quad \frac{h_1}{h_2} > \left(\frac{\rho_2}{\rho_1} \right)^{1/2}, \tag{3.62}$$

$$\lambda_I = \frac{2}{\kappa a_-} \left[(a_+ - a_*)^{1/2} \left(F(\delta_2, m_2) - E(\delta_2, m_2) \right) + (a_+ - a_-) \left(\frac{a_*}{a_- a_+} \right)^{1/2} \right], \quad \text{for} \quad \left(\frac{\rho_1}{\rho_2} \right)^{1/2} < \frac{h_1}{h_2} < \left(\frac{\rho_2}{\rho_1} \right)^{1/2}, \tag{3.63}$$

$$\lambda_I = \frac{2}{\kappa a_+} \left[\left(\frac{a_* a_+}{a_-} \right)^{1/2} - (a_* - a_-)^{1/2} \left(F(\delta_3, m_3) - E(\delta_3, m_3) \right) \right], \quad \text{for} \quad \frac{h_1}{h_2} < \left(\frac{\rho_1}{\rho_2} \right)^{1/2}, \tag{3.64}$$

where F and E are elliptic integrals of the first and second kind (Byrd & Friedman 1954). Here the parameters δ_i, $i = 1, 2, 3$ and m_i, $i = 1, 2$, (cf. (3.59)) are, respectively,

$$\sin\delta_1 = \left[\frac{a_-(a_+ - a_*)}{a_+(a_- - a_*)} \right]^{1/2}, \quad \sin\delta_2 = \left(\frac{a_-}{a_+} \right)^{1/2}, \quad \sin\delta_3 = \left[\frac{a_+(a_- - a_*)}{a_-(a_+ - a_*)} \right]^{1/2}, \tag{3.65}$$

$$m_1^2 = \frac{a_- - a_*}{a_+ - a_*}, \qquad m_2^2 = \frac{a_* - a_+}{a_* - a_-}, \tag{3.66}$$

and the coefficient κ is defined in (3.60).

These expressions for λ_I should be compared with that for KdV solitary waves,

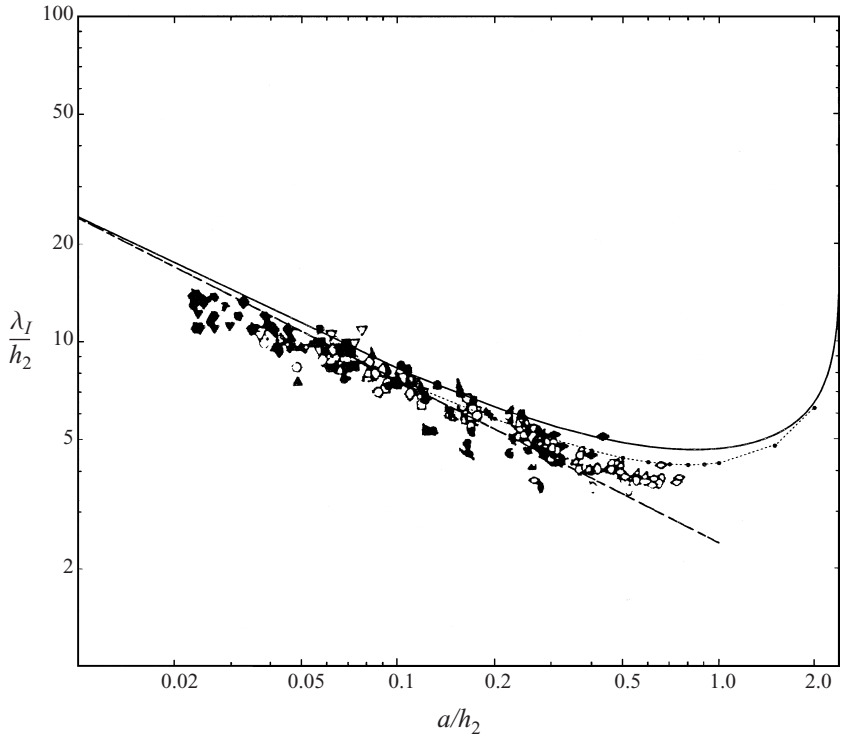

FIGURE 5. Effective wavelength λ_I versus wave amplitude a curves compared with experimental data (symbols, reproduced with permission from Cambridge University Press) by Koop & Butler (1981) for $\rho_1/\rho_2 = 0.63$ and $h_1/h_2 = 5.09$: ——, fully nonlinear theory given by (3.62); – – –, weakly nonlinear (KdV) theory given by (3.67); · · · ● · · ·, numerical solutions of the full Euler equations by Grue *et al.* (1997).

where λ_I is, from (3.38),

$$\lambda_I = \lambda_{KdV} = \left[\frac{4h_1^2h_2^2(\rho_1h_1 + \rho_2h_2)}{3a(\rho_2h_1^2 - \rho_1h_2^2)}\right]^{1/2}. \tag{3.67}$$

We can also compare these results for λ_I with those obtained experimentally by Koop & Butler (1981) within their shallow water configuration, $h_1/h_2 = 5.09$.† Figure 5 shows the experimental data (symbols) vs. theoretical curves from the fully nonlinear (coupled GN) and weakly nonlinear (KdV) theories, equations (3.62) and (3.67), respectively. For $\alpha = a/h_2 < 0.05$, the experimental data lie a little below both theoretical curves, while the data show good agreement with the theoretical predictions for $0.05 < \alpha < 0.2$.

Notice that both the weakly nonlinear and the present fully nonlinear theories are asymptotic approximations to the full Euler equations, and their solutions should approach those of the Euler system as the amplitude a decreases and the effective wavelength λ_I increases, which occurs for the solitary wave solutions of both models.

† Segur & Hammack (1982) examined whether this depth ratio, $\gamma = 5.09$, might be large enough to fall within the domain of asymptotic validity (for small α) of the ILW model. Their answer is negative, a situation only partially remedied by the inclusion of the next higher-order terms in the ILW asymptotic expansion. For more details on higher-order weakly nonlinear unidirectional models, see the Appendix.

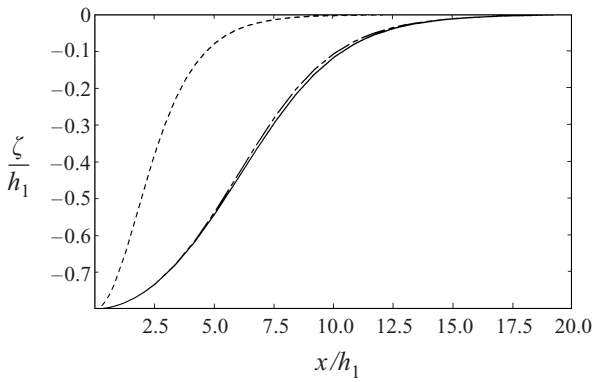

FIGURE 6. Comparison of solitary wave solutions (——) of (3.51) for $\rho_1/\rho_2 = 0.997$, $h_2/h_1 = 3$ and $a/h_1 = -0.8$ compared with KdV solitary waves (– – –) of the same amplitude given by (3.39) and the exact solution of the Euler equations (— – —) computed by Evans & Ford (1996).

Thus the disagreement with the experimental data for $\alpha < 0.05$ could be attributed to the inadequacy, in these regimes, of the Euler system itself. As pointed out by Koop & Butler, for very small waves viscous effects might have to be included.

For larger amplitude of $\alpha > 0.2$, the experimental data lie in between the fully nonlinear and weakly nonlinear results given by (3.62) and (3.67), respectively. It is a little surprising to see that the prediction of the present fully nonlinear theory is as poor as that of the KdV theory based on the weakly nonlinear assumption, though the fully nonlinear model shows the right trend of larger λ_I at given a when compared with KdV.

In order to investigate whether the cause of the discrepancy between the fully nonlinear theory and the experiment by Koop & Butler lies in the approximation of long waves we used to derive the model, we also have compared the present theory with their counterparts from computations using the full Euler equations. As shown in figure 5, the fully nonlinear theory overestimates λ_I for intermediate wave amplitudes compared with numerical solutions of Grue *et al.* (1997), while both theories agree well for large wave amplitudes. Notice that the experimental data by Koop & Butler lie below both theoretical curves. Next we show in figure 6 a plot of our solution vs. that of the solitary wave solution computed numerically by Evans & Ford (1996), for the case (lower layer deeper than the upper layer) $h_1/h_2 = \frac{1}{3}$ and $\rho_1/\rho_2 = 0.997$, i.e. Case (iii) above. The two wave forms for $a/h_1 = -0.8$ are almost identical. Moreover, the wave speed $c/c_0 \approx 1.1486$ from (3.57) is in excellent agreement with their computed value $c/c_0 \approx 1.1485$. Finally, we remark that the maximum values of wave amplitude (and wave speed) at which the solitary wave degenerates into a front match well with those obtained numerically by Evans & Ford (1996).

Therefore, it seems safe to conclude that the discrepancy between the present theory and the experiment depicted by figure 5 when $\alpha > 0.2$ should not be attributed to the long-wave approximation in the model, and it is due to other, at present not easily identifiable, causes. A satisfactory resolution of this issue might have to wait for experimental data in the (extensive) regime of larger waves $0.8 < \alpha < \alpha_m = a_m/h_2 \approx 2.4$, to use the shallow water parameters of Koop & Butler's experiments.

In the remainder of this section, we focus on the limiting case $a \to a_m$ of the highest solitary wave, where, as the phase-space analysis of (3.51) shows, it degenerates into a front-like, or internal bore, solution.

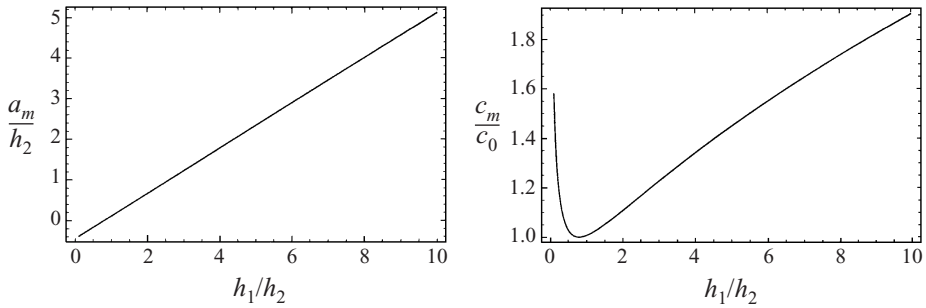

FIGURE 7. Highest wave amplitude and its speed given by (3.68)–(3.69) for $\rho_1/\rho_2 = 0.63$ and varying h_1/h_2.

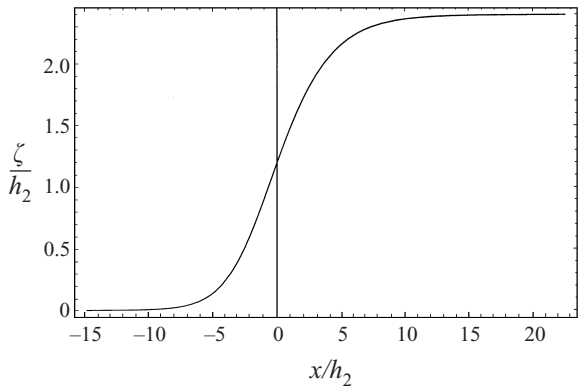

FIGURE 8. A front solution of maximum wave amplitude for $\rho_1/\rho_2 = 0.63$ and $h_1/h_2 = 5.09$.

From (3.55) and (3.57), the amplitude and speed of the highest travelling waves are, for given h_i and ρ_i, $i = 1, 2$,

$$a_m = \frac{h_1 - h_2(\rho_1/\rho_2)^{1/2}}{1 + (\rho_1/\rho_2)^{1/2}}, \tag{3.68}$$

$$c_m^2 = g(h_1 + h_2)\frac{1 - (\rho_1/\rho_2)^{1/2}}{1 + (\rho_1/\rho_2)^{1/2}}. \tag{3.69}$$

Beyond this maximum wave amplitude a_m, no solitary wave solution exists. From (3.68), it is interesting to notice that a_m vanishes at the same critical depth ratio as (3.41) found from the weakly nonlinear analysis. For $\rho_1/\rho_2 = 0.63$ which is the density ratio in the experiment of Koop & Butler (1981), $(h_1/h_2)_c \approx 0.79$ and figure 7 shows a_m and c_m for varying h_1/h_2.

Equation (3.51) at the highest wave of amplitude a_m integrates easily in terms of elementary functions only. The wave profile in this limiting situation is, for the three cases (i)–(iii) respectively,

$$a_m\kappa_m X = \begin{cases} X_f(\zeta, a_m, a_*) - X_f(\zeta_0, 0, a_*) & \text{for } (h_1/h_2) > (\rho_2/\rho_1)^{1/2}, \\ X_f(-\zeta, -a_m, -a_*) - X_f(-\zeta_0, 0, -a_*) & \\ \quad \text{for } (\rho_1/\rho_2)^{1/2} < (h_1/h_2) < (\rho_2/\rho_1)^{1/2}, & \\ -X_f(-\zeta, -a_m, -a_*) + X_f(-\zeta_0, 0, -a_*) & \text{for } (h_1/h_2) < (\rho_1/\rho_2)^{1/2}, \end{cases} \tag{3.70}$$

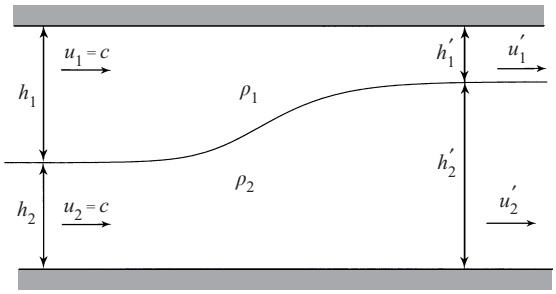

FIGURE 9. Steady flow in a frame moving with a left-going front.

where $\zeta_0 \equiv \zeta(X = 0) = a_m/2$,

$$\kappa_m = \left| \frac{3g(\rho_2 - \rho_1)}{c_m^2(\rho_1 h_1^2 - \rho_2 h_2^2)} \right|^{1/2}, \tag{3.71}$$

and the function X_f is

$$X_f(x, y, z) = (y - z)^{1/2} \log \frac{(x - z)^{1/2} + (y - z)^{1/2}}{(x - z)^{1/2} - (y - z)^{1/2}} - (-z)^{1/2} \log \frac{(x - z)^{1/2} + (-z)^{1/2}}{(x - z)^{1/2} - (-z)^{1/2}}. \tag{3.72}$$

As figure 8 shows, the limiting wave form is a front slowly varying from 0 to a_m.

We remark that for the case of a homogeneous layer, the analogue of the present fully nonlinear model is offered by the GN system given by (3.20) and (3.22) with $P = 0$. Its solitary wave solutions are

$$\zeta(X) = a \operatorname{sech}^2(\kappa_1 X), \quad \kappa_1^2 = \frac{3a}{4(1 + a)}, \quad c^2 = 1 + a, \tag{3.73}$$

and it is interesting to notice that no limiting wave amplitude exists in this case.

Because we have not imposed any assumption on the magnitude of the wave amplitude in order to derive our long-wave model, and since the solution (3.70)–(3.72) is consistent with the long-wave assumption (3.1), it is natural to expect that a similar front solution exists for the full Euler system. In fact, this was demonstrated by Funakoshi & Oikawa (1986), who also used their proof to validate their numerical solutions. For completeness, we now come back to the existence proof of Euler front solutions (rederiving the result of Funakoshi & Oikawa 1986) and compare these to the highest wave solutions of the present long-wave model.

3.4. *Internal bore: exact theory*

We assume the set-up illustrated in figure 9 for an internal bore moving from right to left at constant speed c into a two-layer stratified fluid at rest at $x = -\infty$. Thus, in a frame moving with such a left-going front of speed c, the velocity at $x = -\infty$ is c in both fluids, i.e. $u_1 = u_2 = c$. On the other hand, the velocity at $x = \infty$ can be expected to be different, say u_1' (u_2'), in an upper (lower) fluid layer whose thickness is h_1' (h_2'). The question of existence of front-like solutions is then equivalent to that of finding c, u_i' and h_i' for given ρ_i and h_i, $i = 1, 2$, such that all three basic physical conservation laws of mass, momentum and energy hold.

Mass conservation in each fluid implies

$$ch_1 = u_1' h_1', \qquad ch_2 = u_2' h_2', \tag{3.74}$$

where h_1' and h_2' have to satisfy the geometric constraint

$$h_1 + h_2 = h_1' + h_2'. \tag{3.75}$$

From momentum conservation, the increase of horizontal momentum by momentum flux has to be balanced by the force applied on the boundaries at $x = \pm\infty$. Thus,

$$\rho_1 h_1 c^2 + \rho_2 h_2 c^2 - \rho_1 h_1' {u_1'}^2 - \rho_2 h_2' {u_2'}^2 = \int_{h_1 - h_1'}^{h_1'} p_1 \,\mathrm{d}z + \int_{-h_2'}^{h_2' - h_2} p_2 \,\mathrm{d}z - \int_0^{h_1} p_1 \,\mathrm{d}z - \int_{-h_2}^{0} p_2 \,\mathrm{d}z. \tag{3.76}$$

The pressure p_i can be obtained from the Bernoulli equation,

$$p_i + \tfrac{1}{2}\rho_i (u_i^2 + v_i^2) + \rho_i g z = B_i, \tag{3.77}$$

where the Bernoulli constants B_i are related, by imposing the pressure continuity across the interface at $x = -\infty$, as

$$B_1 - B_2 = \tfrac{1}{2}(\rho_1 - \rho_2) c^2. \tag{3.78}$$

After substituting (3.74)–(3.75) and (3.77) into (3.76), we have

$$(\rho_1 h_1 + \rho_2 h_2) c^2 - \tfrac{1}{2}\rho_1 (h_1 + h_2) c^2 - \tfrac{1}{2}\rho_1 g h_1^2 + \tfrac{1}{2}\rho_2 g h_2^2 = \tfrac{1}{2}\rho_1 h_1' {u_1'}^2 + \tfrac{1}{2}\rho_2 h_2' {u_2'}^2 - \tfrac{1}{2}(\rho_1 - \rho_2) h_2' c^2 + \tfrac{1}{2}\rho_1 g {h_1'}^2 - \tfrac{1}{2}\rho_2 g {h_2'}^2 - \rho_1 g h_1 h_1' + \rho_2 g h_2 h_2'. \tag{3.79}$$

Regarding energy conservation, for steady flows it can be replaced by the Bernoulli theorem. Thus, from the Bernoulli equation (3.77) with (3.78) evaluated at $x = \infty$, we can find one extra condition, after imposing pressure continuity at the interface and substituting (3.74) for u_i':

$$\tfrac{1}{2}\rho_1 c^2 - \tfrac{1}{2}\rho_2 c^2 - \rho_1 g h_1 - \rho_2 g h_2 = \tfrac{1}{2}\rho_1 {u_1'}^2 - \tfrac{1}{2}\rho_2 {u_2'}^2 - \rho_1 g h_1' - \rho_2 g h_2'. \tag{3.80}$$

The final result is the five equations in (3.74)–(3.75) and (3.79)–(3.80) for the five unknowns $(c, h_1', h_2', u_1', u_2')$.

In fact, the approximate theory already contains equations (3.79)–(3.80). These can be obtained by (3.48)–(3.49) evaluated at $X = +\infty$, after imposing $(\eta_{iX}, \eta_{iXX}) \to 0$ and $\zeta \to \zeta_\infty$ as $X \to +\infty$, and using

$$\zeta_\infty = h_1 - h_1' = h_2' - h_2. \tag{3.81}$$

Moreover, by using (3.74)–(3.75) and (3.81), we can obtain an expression for ζ_∞. Multiplying (3.80) by $\zeta_\infty/2$ and subtracting from (3.79) yields

$$\frac{\rho_1}{(h_1 - \zeta_\infty)^2} = \frac{\rho_2}{(h_2 + \zeta_\infty)^2}. \tag{3.82}$$

The solution of (3.82) is $\zeta_\infty = a_m$, so that $c = c_m$, with a_m and c_m given by (3.68) and (3.69), respectively. Thus the Euler equations indeed possess an internal bore solution of the same amplitude and speed as the highest wave amplitude of the long-wave model. Of course, this does not guarantee that the internal bore solution from the long-wave model at intermediate x-values approximates closely the corresponding Euler solutions, though the good agreement with the full Euler computations of Evans & Ford is certainly encouraging.

We conclude this section with a remark on the case of a homogeneous fluid layer, where it is well known that front solutions satisfying all three conservation laws are

impossible. The case of single fluid layer is simply $\rho_1 = 0$. Then the three conservation laws (3.74), (3.79) and (3.80) are

$$ch_2 = u_2'h_2', \quad c^2h_2 - u_2'^2h_2' = \tfrac{1}{2}g(h_2'^2 - h_2^2), \quad \tfrac{1}{2}c^2 + gh_2 = \tfrac{1}{2}u_2'^2 + gh_2', \tag{3.83}$$

and, for given h_2, the only solution is

$$h_2' = h_2, \qquad u_2' = c, \tag{3.84}$$

i.e. a solitary wave rather than a front solution. By only imposing the first two conservation laws for mass and momentum, we have the shock condition for given h_2 and c (Lamb 1932),

$$\frac{h_2'}{h_2} = \frac{1}{2}\left[-1 + \left(1 + \frac{8c^2}{gh_2}\right)^{1/2}\right]. \tag{3.85}$$

The energy loss that this shock solution implies is then attributed to the effects of viscosity, which are large due to the turbulent state at the bore's front.

4. Deep water configuration

4.1. *Fully nonlinear model*

So far we have concentrated on the shallow water configuration $\gamma = O(1)$, whereby propagation of waves in the two-fluid system occurs at a typical wavelength L which is assumed to be large with respect to the undisturbed thickness of both fluid layers. We now turn our attention to the deep water configuration, which we take to be a thin upper layer over a deep layer below, in such a way that

$$h_1/L \ll 1, \qquad h_2/L = O(1). \tag{4.1}$$

From the continuity equation (2.1), we have

$$w_1/u_1 = O(h_1/L) = O(\epsilon), \qquad w_2/u_2 = O(h_2/L) = O(1), \tag{4.2}$$

and, from the boundary condition (2.4) of continuity of normal velocity at $z = \zeta$, it follows that

$$w_2/u_1 = O(\epsilon), \qquad u_2/u_1 = O(\epsilon) \quad \text{at } z = \zeta, \tag{4.3}$$

where we have used $\zeta_x = O(h_1/L) = O(\epsilon)$ with the scaling (4.2). Hence, we find that the correct scaling for long-wave motion in the deep water configuration is

$$u_1/U_0 = O(\zeta/h_1) = O(1), \qquad u_2/U_0 = O(w_1/U_0) = O(w_2/U_0) = O(\epsilon). \tag{4.4}$$

With this in mind, we now proceed to determine asymptotic approximations of the Euler equations governing the fluid velocities and interface displacements in the upper and lower fluid.

For the thin upper fluid layer, the scaling in (4.1) and (4.4) is the same as the one used for the shallow water configuration. Thus, (3.19) and (3.21) are still the governing equations for ζ and $\overline{u}_1$:

$$\zeta_t - [(1-\zeta)\overline{u}_1]_x = 0, \tag{4.5}$$

$$\overline{u}_{1t} + \overline{u}_1\overline{u}_{1x} + \zeta_x = -P_x + O(\epsilon^2). \tag{4.6}$$

Notice that in (4.6) we do not write explicitly the nonlinear dispersive term of $O(\epsilon^2)$ in (3.21), because the leading-order dispersive effect due to the coupling with the deep lower fluid now enters at $O(\epsilon)$, as we shall see presently.

For the lower fluid layer, using the scaling (4.4), we non-dimensionalize all physical variables,

$$\left.\begin{gathered} x = Lx^*, \quad z = Lz^*, \quad t = (L/U_0)t^*, \\ \zeta = h_1\zeta^*, \quad p_2 = \rho_1 U_0^2 p_2^*, \quad u_2 = \epsilon U_0 u_2^*, \quad w_2 = \epsilon U_0 w_2^*, \quad \phi = \epsilon U_0 L\phi^*, \end{gathered}\right\} \tag{4.7}$$

where have introduced the velocity potential ϕ defined by $(\phi_x, \phi_z) = (u_2, w_2)$, assuming the flow in the lower fluid to be irrotational. Comparing (4.7) with (3.3) shows that z is normalized with respect to L since the depth of the lower fluid h_2 is much greater than that of the upper fluid h_1, and it is comparable to the typical wavelength L.

The coupling term P_x in (4.6) follows from the Bernoulli equation evaluated at the interface, which can be written, from the Euler equations (2.2)–(2.3), (after dropping the asterisks) as

$$\epsilon\phi_t + \tfrac{1}{2}\epsilon^2\left(\phi_x^2 + \phi_z^2\right) + \zeta + (\rho_1/\rho_2)P = C(t), \tag{4.8}$$

where $C(t)$ is an arbitrary function of time. Then, up to $O(\epsilon)$, the pressure derivative P_x is

$$P_x = -(\rho_2/\rho_1)\left[\zeta_x + \epsilon\phi_{xt}(x, 0, t)\right] + O(\epsilon^2), \tag{4.9}$$

where we have used $\phi_x(x, \epsilon\zeta, t) = \phi_x(x, 0, t) + O(\epsilon)$. From (2.1) and (2.4)–(2.5), the velocity potential ϕ is a solution of the following boundary value problem:

$$\phi_{xx} + \phi_{zz} = 0 \quad \text{for} \quad -h_2 \leqslant z \leqslant \epsilon\zeta(x, t), \tag{4.10}$$

$$\phi_z = \zeta_t + \epsilon\zeta_x\phi_x \quad \text{at } z = \epsilon\zeta(x, t), \tag{4.11}$$

$$\phi_z = 0 \quad \text{at } z = -h_2. \tag{4.12}$$

As equation (4.9) shows, the linear solution for ϕ is sufficient to determine P_x up to $O(\epsilon)$. Therefore, we first expand (4.11) about $z = 0$,

$$\phi_z = \zeta_t + O(\epsilon) \quad \text{at } z = 0. \tag{4.13}$$

After solving (4.10) for $-h_2 \leqslant z \leqslant 0$ with (4.12)–(4.13) via a Fourier transform, we obtain

$$\phi_x(x, 0, t) = \mathscr{T}_c[\phi_z(x, 0, t)] = \mathscr{T}_c[\zeta_t] + O(\epsilon), \tag{4.14}$$

where the operator $\mathscr{T}_c$ is defined by

$$\mathscr{T}_c[f] = \frac{1}{2h_2} \fint f(x') \coth\left[\frac{\pi}{2h_2}(x' - x)\right] \mathrm{d}x', \tag{4.15}$$

and $\fint$ stands for the integration in the principal value sense. Substituting (4.14) into (4.9) yields

$$P_x = -(\rho_2/\rho_1)(\zeta_x + \epsilon\mathscr{T}_c[\zeta_{tt}]) + O(\epsilon^2). \tag{4.16}$$

Finally, from (4.5)–(4.6), after using (4.16) for P_x, we have the complete set of equations for the displacement of the interface ζ and the depth-mean velocity across the upper layer $\bar{u}_1$. In dimensional form, these are

$$\zeta_t - \left[(h_1 - \zeta)\bar{u}_1\right]_x = 0, \tag{4.17}$$

$$\bar{u}_{1t} + \bar{u}_1\bar{u}_{1x} + \left(1 - \frac{\rho_2}{\rho_1}\right) g\zeta_x = \left(\frac{\rho_2}{\rho_1}\right) \mathscr{T}_c\left[\zeta_{tt}\right]. \tag{4.18}$$

System (4.18)–(4.17) takes the slightly more compact form

$$\eta_{1t} + \left(\eta_1 \overline{u}_1\right)_x = 0, \tag{4.19}$$

$$\overline{u}_{1t} + \overline{u}_1 \overline{u}_{1x} + g\left(\frac{\rho_2}{\rho_1} - 1\right)\eta_{1x} = -\left(\frac{\rho_2}{\rho_1}\right)\mathscr{T}_c\left[\eta_{1tt}\right], \tag{4.20}$$

when using the upper-layer thickness variable $\eta_1 \equiv h_1 - \zeta$. In (4.18) or (4.20), the right-hand-side term should be understood as a shorthand notation, by use of (4.19), for

$$\mathscr{T}_c\left[\zeta_{tt}\right] = -\mathscr{T}_c\left[\eta_{1tt}\right] = \mathscr{T}_c\left[\eta_1 \overline{u}_1\right]_{xt} = \mathscr{T}_c\left[-\overline{u}_1\left(\eta_1 \overline{u}_1\right)_x + \eta_1 \overline{u}_{1t}\right]_x, \tag{4.21}$$

so that only the first time derivative of $\overline{u}_1$ enters the right-hand side of (4.18) or (4.20).

In the limit of infinitely deep lower fluid ($h_2 \to \infty$), the operator $\mathscr{T}_c$ becomes the Hilbert transform $\mathscr{H}$ defined by

$$\mathscr{H}[f] \equiv \frac{1}{\pi} \int \frac{f(x')}{x' - x} \mathrm{d}x', \tag{4.22}$$

and (4.17)–(4.18) reduce to the set of equations derived by Choi & Camassa (1996*b*).

Similarly to the GN equations for the shallow water configuration, the system (4.17)–(4.18) (or, alternatively, system (4.19)–(4.20)) conserves mass, irrotationality, momentum and energy defined by

$$\frac{\mathrm{d}\mathscr{M}}{\mathrm{d}t} \equiv \frac{\mathrm{d}}{\mathrm{d}t} \int \zeta \, \mathrm{d}x = 0, \tag{4.23}$$

$$\frac{\mathrm{d}\mathscr{I}}{\mathrm{d}t} \equiv \frac{\mathrm{d}}{\mathrm{d}t} \int \overline{u}_1 \, \mathrm{d}x = 0, \tag{4.24}$$

$$\frac{\mathrm{d}\mathscr{P}}{\mathrm{d}t} \equiv \frac{\mathrm{d}}{\mathrm{d}t} \int \left(\rho_1 \eta_1 \overline{u}_1 + \rho_2 (h_1 - \eta_1) \mathscr{T}_c[\eta_1 \overline{u}_1]_x\right) \mathrm{d}x = 0, \tag{4.25}$$

$$\frac{\mathrm{d}\mathscr{E}}{\mathrm{d}t} \equiv \frac{\mathrm{d}}{\mathrm{d}t} \left[\frac{1}{2} \int (\rho_2 - \rho_1) g (h_1 - \eta_1)^2 \, \mathrm{d}x + \frac{1}{2} \int \left(\rho_1 \eta_1 \overline{u}_1^2 - \rho_2 \eta_1 \overline{u}_1 \mathscr{T}_c[\eta_1 \overline{u}_1]_x\right) \mathrm{d}x\right] = 0. \tag{4.26}$$

The case of a deep upper layer over a thin lower layer can be readily covered by making the substitutions

$$g \to -g, \qquad \zeta \to -\zeta, \tag{4.27}$$

and interchanging the subscripts 1 and 2 in the evolution equations (4.17)–(4.18). We get

$$\zeta_t + \left[(h_2 + \zeta)\overline{u}_2\right]_x = 0, \tag{4.28}$$

$$\overline{u}_{2t} + \overline{u}_2 \overline{u}_{2x} + \left(1 - \frac{\rho_1}{\rho_2}\right) g \zeta_x = -\left(\frac{\rho_1}{\rho_2}\right) \mathscr{T}_c\left[\zeta_{tt}\right], \tag{4.29}$$

where h_2 has to be replaced by h_1 for the definition of $\mathscr{T}_c$ in (4.15).

4.2. *Weakly nonlinear models*

For weakly nonlinear waves, we impose the additional scaling on the initial conditions

$$\overline{u}_1 / U_0 = O(\zeta / h_1) = O(\alpha), \tag{4.30}$$

with $\alpha \ll 1$, and assume a balance between nonlinear and dispersive effects such as $\alpha = O(\epsilon)$. Hence, in this approximation, the nonlinear dispersive term to be dropped out is $\mathscr{T}_c[\zeta\overline{u}_1]_{xt}$, and system (4.17)–(4.18) reduces to the evolution equations for weakly nonlinear waves (Choi & Camassa 1996*a*):

$$\zeta_t - \left[(h_1 - \zeta)\overline{u}_1\right]_x = 0, \tag{4.31}$$

$$\overline{u}_{1t} + \overline{u}_1\overline{u}_{1x} + \left(1 - \frac{\rho_2}{\rho_1}\right) g\zeta_x = \left(\frac{\rho_2}{\rho_1}\right) \mathscr{T}_c\left[h_1\overline{u}_{1xt}\right], \tag{4.32}$$

which is the counterpart of the Boussinesq equations (3.33)–(3.34) for the shallow water configuration.

For unidirectional waves, (4.31)–(4.32) can be further reduced to the ILW equation (Joseph 1977; Kubota *et al.* 1978)

$$\zeta_t + c_0\zeta_x + c_1\zeta\zeta_x + c_2\mathscr{T}_c[\zeta_{xx}] = 0, \tag{4.33}$$

where the constants c_0, c_1 and c_2 are

$$c_0^2 = gh_1\left(\frac{\rho_2}{\rho_1} - 1\right), \quad c_1 = -\frac{3c_0}{2h_1}, \quad c_2 = \frac{c_0\rho_2 h_1}{2\rho_1}. \tag{4.34}$$

The same equation holds for $\overline{u}_1$ at this order of approximation. The ILW equation admits the one-parameter (β) family of solitary wave solutions (Joseph 1977)

$$\zeta_{ILW}(X) = \frac{a\cos^2\beta}{\cos^2\beta + \sinh^2(X/\lambda_{ILW})}, \qquad X = x - ct, \tag{4.35}$$

where

$$a = \frac{4c_2}{h_2c_1}\beta\tan\beta, \quad \lambda_{ILW} = \frac{h_2}{\beta}, \quad c = c_0 - \frac{2c_2}{h_2}\beta\cot(2\beta), \quad 0 \leqslant \beta < \tfrac{1}{2}\pi. \tag{4.36}$$

As $h_2 \to \infty$ and $\beta \to \frac{1}{2}\pi$, (4.35) reduces to the BO solitary wave (Benjamin 1967):

$$\zeta_{BO}(X) = \frac{a}{1 + (X/\lambda_{BO})^2}, \qquad X = x - ct, \tag{4.37}$$

where

$$\lambda_{BO} = \frac{4c_2}{ac_1}, \qquad c = c_0 + \frac{c_1}{4}a. \tag{4.38}$$

For a fixed h_2, as $\beta \to 0$, (4.35) becomes the classical KdV solitary wave:

$$\zeta_{KdV}(X) = a\,\mathrm{sech}^2(X/\lambda_{KdV}), \qquad X = x - ct, \tag{4.39}$$

where

$$\lambda_{KdV}^2 = \frac{4h_2c_2}{ac_1}, \quad c = \left(c_0 - \frac{c_2}{h_2}\right) + \frac{c_1}{3}a. \tag{4.40}$$

The same result expressed by (4.39)–(4.40) follows from (3.39)–(3.40) by taking the limit of large h_2.

For small-amplitude waves, the linear dispersion relation of the bidirectional model (4.31)–(4.32),

$$c^2 = \frac{gh_1(\rho_2 - \rho_1)}{\rho_1 + \rho_2(kh_1)\coth(kh_2)}, \tag{4.41}$$

reduces, by using

$$\mathscr{T}_c[\mathrm{e}^{\mathrm{i}kx}] = \mathrm{i}\coth(kh_2)\,\mathrm{e}^{\mathrm{i}kx}, \tag{4.42}$$

to that for the ILW in equation (2.8) in the limit of small kh_1.

4.3. *Travelling wave solutions*

To compare travelling wave solutions with the experiment by Koop & Butler (1981) for the deep water configuration of thin lower and deep upper fluid layers, we solve (4.28)–(4.29), non-dimensionalized by h_2 and c_0 for the interface ζ and velocity $\overline{u}_2$ variables respectively, with $c_0^2 \equiv gh_2(1-\rho_1/\rho_2)$.

For waves of finite amplitude travelling with constant speed c, we assume that

$$\zeta(x,t) = \zeta(X), \qquad \overline{u}_2(x,t) = \overline{u}_2(X), \qquad X = x - ct. \tag{4.43}$$

After substituting (4.43) into (4.28)–(4.29) and integrating once, we have

$$-c\zeta + (1+\zeta)\overline{u}_2 = C_1, \tag{4.44}$$

$$-c\overline{u}_2 + \tfrac{1}{2}\overline{u}_2^2 + \zeta = -c^2(\rho_1/\rho_2)\mathscr{T}_c[\zeta_X] + C_2, \tag{4.45}$$

where the integration constants C_1 and C_2 are taken to be zero, thereby fixing the mean level. Substituting $\overline{u}_2 = c\zeta/(1+\zeta)$ into (4.45) from (4.44) yields a single equation for ζ:

$$\mathscr{G}[\zeta] \equiv \frac{1}{c^2}\zeta + \frac{1}{2}\frac{1}{(1+\zeta)^2} + \left(\frac{\rho_1}{\rho_2}\right)\mathscr{T}_c[\zeta_X] - \frac{1}{2} = 0. \tag{4.46}$$

Because of the non-local operator $\mathscr{T}_c$ in (4.46), we have not been able to find closed-form travelling wave solutions. Therefore, we have resorted to numerics for finding ζ iteratively via the Newton–Raphson method. First, we assume

$$\zeta(X) = \zeta^0(X) + \Delta(X), \tag{4.47}$$

where ζ^0 is the initial guess (or the result from the previous iteration) and Δ is the correction to be found. By substituting (4.47) into (4.46) and linearizing with respect to Δ, we can find the equation for Δ as

$$M[\zeta^0;c]\Delta \equiv \left[-\frac{1}{c^2} + \frac{1}{(1+\zeta^0)^3} - \left(\frac{\rho_1}{\rho_2}\right)\partial_X\mathscr{T}_c\right]\Delta = \mathscr{G}[\zeta^0] + O(\Delta^2). \tag{4.48}$$

With the representation of Δ in terms of discrete Fourier (cosine) series of N-modes, (4.48) evaluated at $X = X_i = i\lambda/N$ $(i = 1,\ldots,N)$ equation (4.48) can be written as

$$M_{ij}\,\Delta_j = -\mathscr{G}_i, \tag{4.49}$$

where $\Delta_j = \Delta(X_j)$, $\mathscr{G}_i = \mathscr{G}[\zeta^0(X_i)]$ and M_{ij} is an element of $N \times N$ matrix resulting from the discretization of the operator $M[\zeta^0;c]$.

In order to find M_{ij} and $\mathscr{G}_i$ in equation (4.49), we use the pseudo-spectral method based on the fast Fourier transform (FFT). By taking the wave speed c as a parameter for given wavelength λ and choosing the solitary wave solution of the ILW equation given by (4.35) as the initial guess for small $c-1$, we solve the linear algebraic equation (4.48) for Δ_j iteratively until $\max(\Delta_j)$ is smaller than the error bound e. We then proceed to find the solution for a larger $c-1$ by taking the previous results for $c-1$ as the initial guess. (An alternative method is to fix the wave amplitude for a given wavelength.) For travelling waves close to solitary waves, we take a large wavelength λ (typically $\lambda = 400$), with $N = 2^7 = 128$ and $e = 10^{-6}$ for our computations.

We show some typical results in figure 10. As for the shallow water configuration in § 3.3, the travelling waves of finite amplitude found numerically are wider than the weakly nonlinear ILW solitary waves of the same speed (4.35). Likewise, the speed of fully nonlinear waves increases with amplitude at a much slower rate than the weakly nonlinear ILW theory, as seen in figure 11.

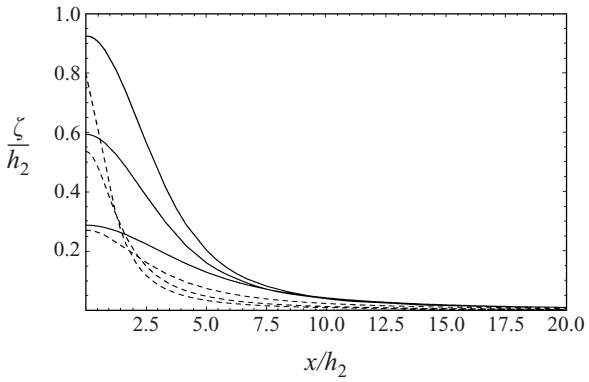

FIGURE 10. Solitary wave solutions (——) of (4.46) for $\rho_1/\rho_2 = 0.63$, $h_1/h_2 = 35.05$ and c/c_0 =(1.1, 1.2, 1.3) compared with ILW solitary waves (– – –) of the same wave speed given by (4.35).

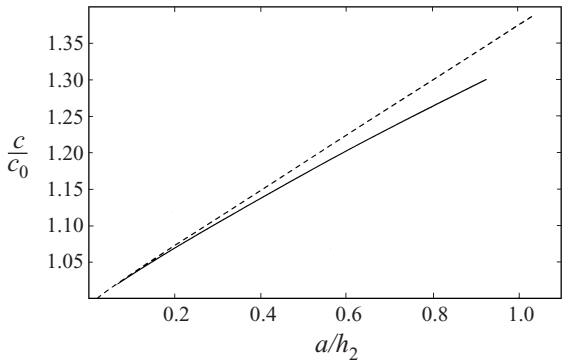

FIGURE 11. Wave speed c versus wave amplitude a for $\rho_1/\rho_2 = 0.63$ and $h_1/h_2 = 35.05$: ——, numerical solutions of (4.46); – – –, weakly nonlinear (ILW) theory given by (4.36).

Similarly to the shallow water case in § 3.3, we also compute the effective wavelength λ_I defined by (3.61), in order to compare with the measurements by Koop & Butler (1981). They used the same fluids as in the shallow water case, while the thickness ratio for the deep water configuration was set at $h_1/h_2 = 35.05$. For weakly nonlinear theories, λ_I can easily be found,

$$\lambda_I = \begin{cases} \lambda_{KdV} & \text{KdV theory} \\ h_1 \cot(h_1/\lambda_{ILW}) & \text{ILW theory} \\ \frac{1}{2}\pi\lambda_{BO} & \text{BO theory,} \end{cases} \tag{4.50}$$

where λ_{KdV}, λ_{ILW} and λ_{BO} are defined by (3.67), (4.36) and (4.38), for the KdV, ILW and BO equations, respectively. Among these three weakly nonlinear equations, the most appropriate for $h_1/h_2 = 35.05$ is expected to be the ILW theory. As figure 12 shows, the experimental data intersect the curve provided by the ILW model around the amplitude $\alpha = a/h_2 = 0.1$. For both smaller $0.02 < \alpha < 0.1$ and larger $0.15 < \alpha < 0.65$ amplitudes the ILW curve fails to represent the data, and clearly exhibit an incorrect slope throughout the data set. However, the regimes for small-amplitude data should fulfil the assumptions for the asymptotic derivation of the ILW model based on weak nonlinearity with the scaling $\alpha = O(\epsilon)$. Hence, the shortcomings already encountered in the shallow water configuration occur for the deep water case as well, and in a

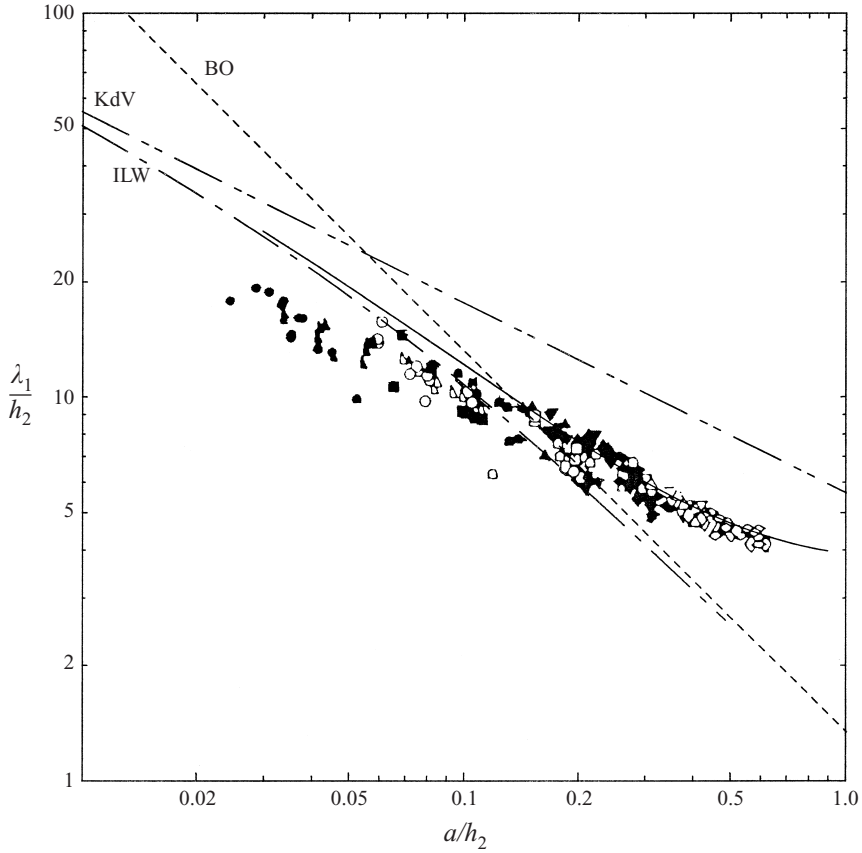

FIGURE 12. Effective wavelength λ_I versus wave amplitude a curves compared with experimental data (symbols, reproduced with permission from Cambridge University Press) by Koop & Butler (1981) for $\rho_1/\rho_2 = 0.63$ and $h_1/h_2 = 35.05$: ——, fully nonlinear theory given by (4.46); — - —, KdV model (3.67); — -- —, ILW model (4.35); – – –, BO model (4.37).

more severe form. Once again, the discrepancy between model and data cannot be immediately attributed to limitations of the ILW model.

Conversely, the observed discrepancy for larger amplitudes waves, with $0.15 < \alpha < 0.65$, could indeed signal that the ILW equation is being applied outside its domain of asymptotic validity, and that a new theory needs to be introduced for this regime. The agreement between the present theory and experimental data in figure 12 is remarkably good for $0.2 < \alpha < 0.65$, while the curve from recent numerical solutions of the full Euler equations by Laget & Dias (1997) lies slightly above the experimental data. From this comparison, we can conclude that the weak nonlinearity assumption $\alpha = O(\epsilon)$ is the principal cause of discrepancy between theory and experiments in these regimes.

4.4. *Evolution of solitary waves*

Owing to their simple forms, the models derived here are much easier to use than the original Euler equations in studying the evolution of finite-amplitude waves. With the help of a straightforward numerical scheme, we solve system (4.28)–(4.29) to study the interaction of solitary waves in deep water.

Throughout our numerical computations, we use the pseudo-spectral method in

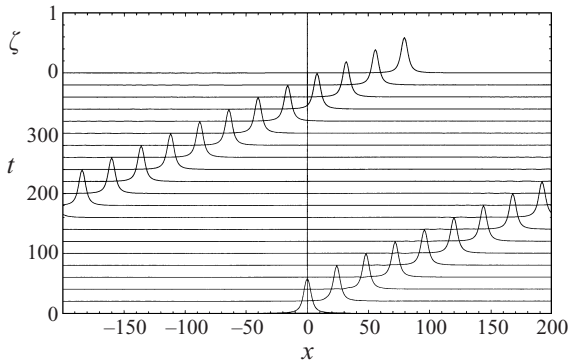

FIGURE 13. Numerical solutions of (4.28)–(4.29) for the propagation of a single solitary wave of $c/c_0 = 1.2$.

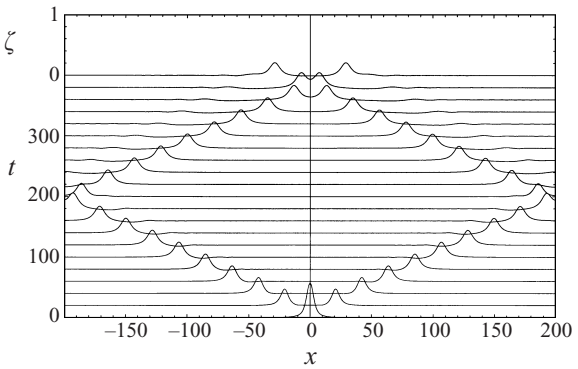

FIGURE 14. Numerical solutions of (4.28)–(4.29) for the fission of a single solitary wave of $c/c_0 = 1.2$ with $\bar{u}_2(x,0) = 0$.

space with a number of Fourier modes $N = 2^8 = 256$ and the fourth-order Runge–Kutta time-integration scheme with increment $\Delta t = 0.5$. For definiteness, we keep the parameter values of Koop & Butler's experiment, $h_1/h_2 = 35.05$ and $\rho_1/\rho_2 = 0.63$. We first validate the numerical code by taking as initial conditions the solutions for travelling waves found in § 4.3. Figure 13 confirms that the travelling wave solution of $c/c_0 = 1.2$ ($a/h_2 \approx 0.579$) travels with no appreciable change in shape and furthermore appears to be stable to numerical disturbances.

Next, by taking an initial hump given by the $\zeta(x,0)$ component of the travelling wave solution, and setting $\bar{u}_2(x,0) = 0$, we simulate the fission of a solitary wave, as shown in figure 14. The initial hump at $x = 0$ evolves into two solitary waves propagating in opposite directions and colliding with waves coming from adjacent computation periods.

Finally, we consider collisions of two solitary waves in the form of overtaking and head-on, as shown in figures 15 and 16. The generation of small trailing waves after collision indicates that the interaction is inelastic and solitary waves for this system are not likely to behave as solitons. Figures 17 and 18 depict the history of the peak positions for the interacting solitary waves in the overtaking and head-on collision of figures 15 and 16, respectively. Although it is very small, a phase shift due to the nonlinear interaction during the overtaking collision can be clearly seen in figure 17;

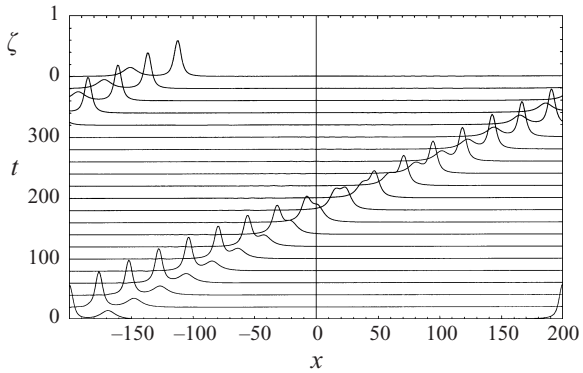

FIGURE 15. Numerical solutions of (4.28)–(4.29) for the overtaking collision of two different solitary waves. Initially the larger solitary wave of $c/c_0 = 1.2$ ($a/h_2 \approx 0.579$) is located at $x = -200$ and the smaller wave of $c/c_0 = 1.05$ ($a/h_2 \approx 0.147$) at $x \approx -170$.

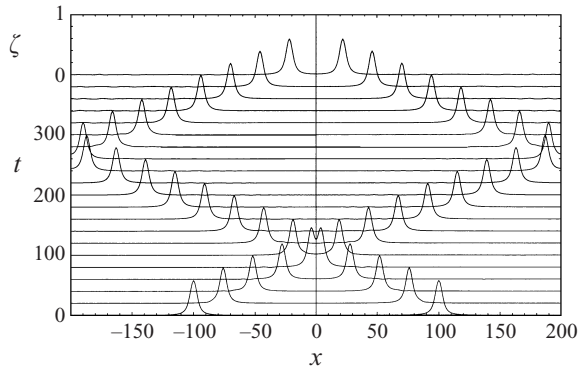

FIGURE 16. Numerical solutions of (4.28)–(4.29) for the head-on collision of two identical solitary waves of $c/c_0 = 1.2$, initially located at $x = \pm 100$, propagating in opposite directions.

it is such that the faster (taller) solitary wave emerges ahead of where it would be without collision, while the slower (shorter) wave is delayed by the interaction. For the head-on collision case, close examination of figure 18 reveals the analogous phase shift where the peak of each solitary wave finds itself behind the position it would have occupied if the interaction did not occur.

5. Discussion

For small aspect ratio of the thickness of the upper fluid layer to typical wavelength, we have derived fully nonlinear models to describe the evolution of finite-amplitude long internal waves in a two-fluid system for both shallow and deep water configurations. These models retain much of the structural simplicity of the classical weakly nonlinear models, while extending substantially their domain of asymptotic validity. In particular, since we impose no condition on the scaling between α and ϵ and only require $\epsilon \ll 1$, we expect solutions of these model equations to automatically select the correct scaling laws depending on a given wave amplitude. For solitary waves, this scaling results in waves that are much wider and whose speed increases at a much slower rate compared with their weakly nonlinear counterparts. We remark

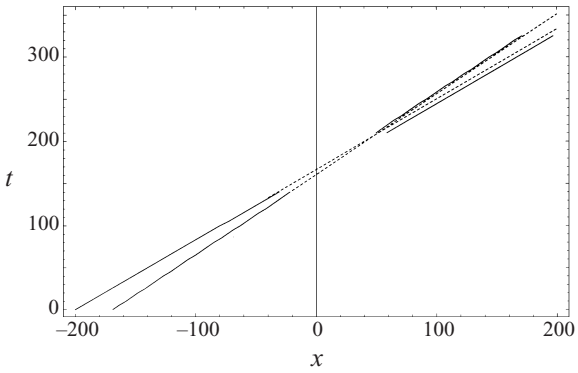

FIGURE 17. Peak locations vs. time for the overtaking collision of two solitary waves shown in figure 15. Dashed lines (– – –) represent the peak location without interaction.

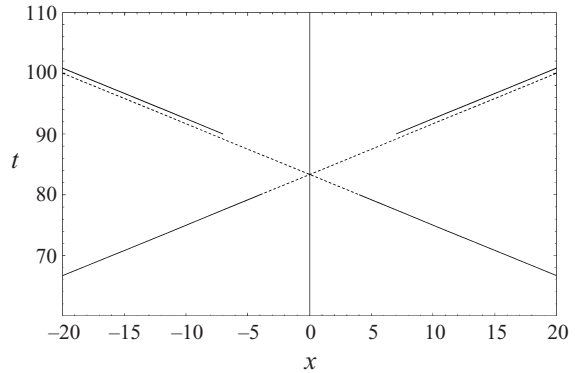

FIGURE 18. Peak locations vs. time for the head-on collision of two solitary waves shown in figure 16. Dashed lines (– – –) represent the peak location without interaction. Notice the difference in scale with respect to figure 17.

that similar trends were also detected for internal solitary waves in continuously stratified fluids, as described by Tung, Chan & Kubota (1982) numerically and Davis & Acrivos (1967) experimentally.

For small-amplitude waves, as pointed out by Koop & Butler (1981), the effects of viscosity seem to become important in selecting a scaling law between wave amplitude and typical wavelength λ_I for both shallow and deep water configurations. Therefore models for small-amplitude waves need to be based on Navier–Stokes, rather than Euler, equations in order to properly account for energy dissipation. An investigation on the interplay among nonlinearity, dispersion and viscosity in this regime is in progress.

For the shallow water configuration, while our fully nonlinear theory does exhibit the qualitative behaviour observed in previous numerical solutions and experiments, and agrees extremely well with high-accuracy numerical solutions of Euler equations, there remains a discrepancy for waves of large amplitude between the λ_I from the theory and the λ_I from the experimental data by Koop & Butler (1981). Because of the closeness of the model's solutions to the numerical solutions of Euler equations (Evans & Ford 1996), this discrepancy should not be attributed to the long-wave approximation in the model, and hence we are at present unable to explain it. More

extensive comparisons between our long-wave theory and experiments are needed before a definite conclusion can be reached.

In § 3.3, we have looked at the limit of the highest solitary wave for our model in the form of an internal bore. We demonstrated the existence of such internal bore solutions of the full Euler equations in § 3.4. However, we are not aware of a theoretical investigation, within the Euler system, of the process by which solitary waves limit to internal bores as the wave amplitude approaches its maximum. It would be interesting to observe this process experimentally, a task that is linked to the theoretical question of stability of finite-amplitude solitary waves.

For the deep water configuration, the fully nonlinear solitary wave solutions of our long-wave model show good agreement with the available experimental data λ_I vs. a. This indicates that the slight overprediction of the theory by Choi & Camassa (1996*b*) is due to the infinite-depth assumption therein.

We thank Y. Matsuno, A. R. Osborne and T. Y. Wu for their remarks and for providing some of the references in the literature. We also thank the reviewer for pointing out the work by Grue *et al.* (1997) and J. Grue and P. O. Rusas for providing the data in figure 5. This work was supported in part by the DOE programs CHAMMP and BES under the Applied Mathematical Sciences contract KC-07-01-01.

Appendix A. Unidirectional models

Models (3.19)–(3.22) and (4.17)–(4.18) for, respectively, shallow and deep water configurations, can describe waves propagating in both x-directions. Thus, these models are of particular relevance whenever counter-propagating waves are an important aspect of the wave dynamics, such as e.g. reflections from a rigid boundary. However, in situations where most of the waves propagate in one direction, as in the case of a solitary wave in an unbounded domain, it should be possible to simplify the models further. In particular, the assumption of unidirectional wave propagation results in a relation between the velocity $\overline{u}_1$ and the free-surface location ζ which reduces bidirectional systems of the type (3.19)–(3.22) and (4.17)–(4.18) to a single model equation for either $\overline{u}_1$ or ζ.

Naturally, it would be desirable to have unidirectional models for waves of finite amplitude, asymptotically equivalent to bidirectional models (3.19)–(3.22) for shallow water or (4.17)–(4.18) for the deep water, respectively. However, we have not succeeded in this task yet. Instead, in this Appendix we adopt a weakly nonlinear assumption while using an ordering between the small nonlinearity parameter α and the long-wave parameter ϵ that emphasizes nonlinearity. In contrast to the classical weakly dispersive shallow water theory, where a single scaling parameter is introduced by imposing $\alpha = \epsilon^2$ and $\alpha = \epsilon$ for, respectively, the shallow and deep water configurations, we will only require

$$\epsilon^2 < \alpha < \epsilon \quad (\text{or } \alpha^2 < \epsilon^2 < \alpha), \tag{A 1}$$

and, for deep water,

$$\epsilon < \alpha < \epsilon^{1/2} \quad (\text{or } \alpha^2 < \epsilon < \alpha), \tag{A 2}$$

with $\epsilon \ll 1$. Since the classical scaling between α and ϵ is $\alpha = O(\epsilon^2)$ for KdV and $\alpha = O(\epsilon)$ for ILW regimes, the new scalings in (A 1)–(A 2) imply that we are interested in waves of larger amplitude than those described by weakly nonlinear models such as the KdV and ILW equations. Therefore, the new unidirectional models are expected to

contain higher-order nonlinear terms and nonlinear dispersive terms. To derive these models, we follow the procedure of Whitham (1974, § 13.11) for the KdV equation.

(i) *Shallow water configuration*

After all physical variables in (3.19)–(3.22) are non-dimensionalized as

$$\zeta = \alpha h_1 \zeta^*, \quad (\overline{u}_1, \overline{u}_2) = \alpha U_0 (\overline{u}_1^*, \overline{u}_2^*), \quad x = L x^*, \quad t = (L/U_0) t^*, \tag{A 3}$$

we assume the relationship between ζ and $\overline{u}_1$, after dropping the asterisks as before, as

$$\zeta = A_0 \overline{u}_1 + \alpha A_1 \overline{u}_1^2 + \epsilon^2 A_2 \overline{u}_{1xt} + \alpha^2 F_1 + \alpha \epsilon^2 F_2 + O(\epsilon^4, \alpha^3, \alpha^2 \epsilon^2). \tag{A 4}$$

In (A 4), F_1 is a cubic function of $\overline{u}_1$ for the higher-order nonlinearity and F_2 represents nonlinear dispersive effects so that

$$F_1 = A_3 \overline{u}_1^3, \qquad F_2 = A_4 \overline{u}_{1x}^2 + A_5 \overline{u}_1 \overline{u}_{1xx}. \tag{A 5}$$

One can see later that, by using (A 4) without $F_i\,(i = 1, 2)$, the procedure described below results in the classical KdV equation (3.37).

Following Whitham (1974), we determine constants the A_i such that, when we substitute the expression (A 4) for ζ, we find the same evolution equation for $\overline{u}_1$, up to $O(\alpha\epsilon^2)$, from any equation of (3.19)–(3.22). After a lengthy manipulation, the coefficients A_i evaluate to (in dimensional form)

$$\left.\begin{aligned} &A_0 = -\frac{h_1}{c_0}, \quad A_1 = -\frac{h_1}{c_0^2}\left(1 + \frac{h_1 c_1}{2c_0}\right), \quad A_2 = -\frac{h_1 c_2}{c_0^3}, \\ &A_3 = \frac{h_1^3 c_3}{c_0^4} - \frac{h_1^3 c_1^2}{2c_0^5} - \frac{3h_1^2 c_1}{2c_0^4} - \frac{h_1}{c_0^3}, \\ &A_4 = -\frac{h_1^2 c_4}{c_0^3} + \frac{2h_1^2 c_1 c_2}{c_0^4} + \frac{2h_1 c_2}{c_0^3}, \quad A_5 = -\frac{h_1^2 c_5}{c_0^3} + \frac{3h_1^2 c_1 c_2}{c_0^4} + \frac{3h_1 c_2}{c_0^3}, \end{aligned}\right\} \tag{A 6}$$

where c_0, c_1 and c_2 are given by (3.38), reported here for convenience,

$$\left.\begin{aligned} &c_0^2 = \frac{g h_1 h_2 (\rho_2 - \rho_1)}{\rho_1 h_2 + \rho_2 h_1}, \quad c_1 = -\frac{3c_0}{2} \frac{\rho_1 h_2^2 - \rho_2 h_1^2}{\rho_1 h_1 h_2^2 + \rho_2 h_1^2 h_2}, \\ &c_2 = \frac{c_0}{6} \frac{\rho_1 h_1^2 h_2 + \rho_2 h_1 h_2^2}{\rho_1 h_2 + \rho_2 h_1}, \end{aligned}\right\} \tag{A 7a}$$

and

$$\left.\begin{aligned} &c_3 = \frac{7c_1^2}{18c_0} - \frac{c_0(\rho_1 h_2^3 + \rho_2 h_1^3)}{h_1^2 h_2^2 (\rho_1 h_2 + \rho_2 h_1)}, \quad c_4 = \frac{17 c_1 c_2}{12 c_0} + \frac{c_0 h_1 h_2 (\rho_1 - \rho_2)}{12(\rho_1 h_2 + \rho_2 h_1)}, \\ &c_5 = \frac{7c_1 c_2}{3c_0} + \frac{c_0 h_1 h_2 (\rho_1 - \rho_2)}{6(\rho_1 h_2 + \rho_2 h_1)}. \end{aligned}\right\} \tag{A 7b}$$

Then the evolution equation for $\overline{u}_1$ is given, in dimensional form, by

$$\overline{u}_{1t} + \gamma_0 \overline{u}_{1x} + \gamma_1 \overline{u}_1 \overline{u}_{1x} + \gamma_2 \overline{u}_{1xxt} + \gamma_3 (\overline{u}_1^3)_x + \left(\gamma_4 \overline{u}_{1x}^2 + \gamma_5 \overline{u}_1 \overline{u}_{1xx}\right)_x = 0, \tag{A 8}$$

where the γ_i are given by

$$\gamma_0 = c_0, \quad \gamma_1 = -\frac{h_1 c_1}{c_0}, \quad \gamma_2 = -\frac{c_2}{c_0},$$

$$\gamma_3 = \frac{h_1^2 c_3}{c_0^2} - \frac{1}{6}\frac{h_1^2 c_1^2}{c_0^3} - \frac{1}{3}\frac{h_1 c_1}{c_0^2},$$

$$\gamma_4 = -\frac{h_1 c_4}{c_0} + \frac{3}{2}\frac{h_1 c_1 c_2}{c_0^2} + \frac{3c_2}{c_0}, \quad \gamma_5 = -\frac{h_1 c_5}{c_0} + \frac{h_1 c_1 c_2}{c_0^2}.$$

By inverting (A 4) to find the expression for $\overline{u}_1$ in terms of ζ and substituting into (A 8), the evolution equation for ζ asymptotically equivalent to (A 8) can be found as

$$\zeta_t + c_0\zeta_x + c_1\zeta\zeta_x + c_2\zeta_{xxx} + c_3\left(\zeta^3\right)_x + \left(c_4\zeta_x^2 + c_5\zeta\zeta_{xx}\right)_x = 0. \tag{A 9}$$

The evolution equation (A 8) or (A 9) is the KdV equation modified by a higher-order nonlinear term of $O(\alpha^2)$ and nonlinear dispersive terms of $O(\alpha\epsilon^2)$.

If we neglect nonlinear dispersive terms (and so set $c_4 = c_5 = 0$), (A 9) becomes a combination of the KdV and modified KdV equation (which has cubic, as opposed to quadratic for KdV) nonlinearity. Notice that such an equation has been derived by several authors by using an asymptotic expansion designed for the case of near-critical depth ratio h_1/h_2 given by (3.41). The present derivation does not make explicit use of this assumption, and hence the coefficients of the extra nonlinear terms differ from the ones for the near-critical regime (see e.g. Funakoshi & Oikawa 1986).

If we impose the balance between nonlinear and dispersive effects, say $\alpha = O(\epsilon^2)$, and want to keep all second-order terms, we need to add to (A 9) the higher-order linear dispersive term of $O(\epsilon^4)$

$$c_6\zeta_{xxxxx}, \qquad c_6 = \frac{3c_2^2}{2c_0} + \frac{c_0 h_1 h_2(\rho_1 h_1^3 + \rho_2 h_2^3)}{90(\rho_1 h_2 + \rho_2 h_1)}. \tag{A 10}$$

With this term (A 9) is sometimes referred to as the second-order KdV equation (Koop & Butler 1981).

Equations (A 8) and (A 9) conserve a mass-like integral, defined either as $\int_{-\infty}^{+\infty}\overline{u}_1\,\mathrm{d}x$ or as $\int_{-\infty}^{+\infty}\zeta\,\mathrm{d}x$ for (A 8) and (A 9), respectively. However, these models do not seem to admit a conservation law that contains the energy-like variables ${\overline{u}_1}^2$ or ζ^2. Lack of an extra conservation law besides the mass also makes it difficult to compute a travelling wave solution in closed form. It is possible however to make use of the leading-order terms in these equations to recombine the asymptotic expansion so as to obtain models which possess an energy conservation law. From the leading-order terms of (A 8), we have

$$\overline{u}_{1xxt} + c_0\overline{u}_{1xxx} + \tfrac{1}{2}c_1(\overline{u}_1^2)_{xxx} = O(\epsilon^2). \tag{A 11}$$

By multiplying (A 11) by an arbitrary constant and adding it to (A 8), many different models asymptotically equivalent to (A 8) can be constructed. Among these models, the particular form

$$\overline{u}_{1t} + \gamma_0\overline{u}_{1x} + \gamma_1\overline{u}_1\overline{u}_{1x} + \left(\gamma_2 + \frac{2\gamma_4 - \gamma_5}{\gamma_1}\right)\overline{u}_{1xxt} + \frac{\gamma_0(2\gamma_4 - \gamma_5)}{\gamma_1}\overline{u}_{1xxx} + \gamma_3\left(\overline{u}_1^3\right)_x + (\gamma_5 - \gamma_4)\left(\overline{u}_{1x}^2 + 2\overline{u}_1\overline{u}_{1xx}\right)_x = 0, \tag{A 12}$$

conserves the following integral:

$$\mathscr{E} = \frac{1}{2}\int_{-\infty}^{+\infty}\left[\overline{u}_1^2 - \left(\gamma_2 + \frac{2\gamma_4 - \gamma_5}{\gamma_1}\right)\overline{u}_{1x}^2\right]\mathrm{d}x. \tag{A 13}$$

Similarly, the following evolution equation for ζ:

$$\zeta_t + c_0\zeta_x + c_1\zeta\zeta_x + \left(\frac{2c_4 - c_5}{c_1}\right)\zeta_{xxt} + \left(c_2 + \frac{c_0(2c_4 - c_5)}{c_1}\right)\zeta_{xxx} + c_3\left(\zeta^3\right)_x + (c_5 - c_4)\left(\zeta_x^2 + 2\zeta\zeta_{xx}\right)_x = 0, \quad \text{(A 14)}$$

conserves

$$\mathscr{E} = \frac{1}{2}\int_{-\infty}^{+\infty}\left[\zeta^2 - \left(\frac{2c_4 - c_5}{c_1}\right)\zeta_x^2\right]\mathrm{d}x. \quad \text{(A 15)}$$

Travelling wave solutions of (A 14) with $X = x - ct$ can be computed by quadratures thanks to the existence of this conservation law. For solitary waves, equation (A 14) reduces to

$$\zeta_X{}^2 = C_u\frac{\zeta^2(\zeta - \tilde{a}_+)(\zeta - \tilde{a}_-)}{\zeta - \tilde{a}_*}, \quad \text{(A 16)}$$

where the coefficient C_u is

$$C_u = \frac{c_3}{4(c_4 - c_5)},$$

the denominator's root $\tilde{a}_*$ is

$$\tilde{a}_* = \frac{c_2(c_4 - c_5) + (c_0 - c)(2c_4 - c_5)}{2c_1(c_4 - c_5)},$$

and $\tilde{a}_\pm$ are the roots of the quadratic equation

$$\zeta^2 + \frac{4}{3}\frac{c_1}{c_3}\zeta + 2\frac{c_0 - c}{c_3} = 0,$$

respectively. Notice the structural similarity of equation (A 16) with that of (3.50) for the solitary wave solutions of the Green–Naghdi system, i.e. $\zeta_X{}^2$ is given by the ratio of a quartic and a linear polynomial in ζ. Hence, $\zeta(X)$ is determined implicitly via elliptic integrals similar to (3.58). Compared to the solutions of the Green–Naghdi system (3.50), the solitary wave solutions of (A 16) are better approximations than their KdV or modified KdV counterparts, over a broad range of parameter values in the shallow water configuration (away from the critical depth ratio (3.41)). Given the excellent agreement between the analogous solutions of the Green–Naghdi and Euler systems, it seems likely that nonlinearity effects of the original system can be rendered more accurately by unidirectional equations of the type (A 14), while maintaining the simplicity of their classic weakly nonlinear counterparts. Of course, complete integrability of (some of) the classic weakly nonlinear models makes them important objects from a mathematical point of view. It is unknown at the moment whether this feature is present in any of the higher-order models.

(ii) *Deep water configuration*

By following a procedure similar to the one above for the shallow water configuration using the scaling law given by (A 2), we can derive the unidirectional model for the deep water case from (4.17)–(4.18) non-dimensionalized by

$$\zeta = \alpha h_1\zeta^*, \quad \overline{u}_1 = \alpha c_0\overline{u}_1^*, \quad x = Lx^*, \quad t = (L/c_0)t^*, \quad \text{(A 17)}$$

where $c_0^2 = gh_1(\rho_2/\rho_1 - 1)$. First, we assume a relation between ζ and $\overline{u}_1$,

$$\zeta = A_1\overline{u}_1 + \alpha A_2\overline{u}_1^2 + \epsilon A_3\mathscr{T}_c[\overline{u}_{1t}] + \alpha^2 F_1 + \alpha\epsilon F_2 + O(\epsilon^2, \alpha^3, \alpha^2\epsilon). \tag{A 18}$$

As before, we determine the A_i and F_i such that, when (A 18) is substituted for ζ, both (4.17) and (4.18) yield the same evolution equation up to $O(\alpha\epsilon)$. The results are given by

$$A_1 = -1, \quad A_2 = -\tfrac{1}{4}, \quad A_3 = -\tfrac{1}{2}(\rho_2/\rho_1),$$

$$F_1 = 0, \quad F_{2x} = \left(\rho_2/\rho_1\right)\left(\tfrac{5}{16}\mathscr{T}_c[\overline{u}_1^2]_{xx} + \tfrac{1}{4}\overline{u}_{1x}\mathscr{T}_c[\overline{u}_{1x}] + \tfrac{3}{8}\overline{u}_1\mathscr{T}_c[\overline{u}_{1xx}]\right).$$

The evolution equation for $\overline{u}_1$ is then

$$\overline{u}_{1t} + \overline{u}_{1x} + \tfrac{3}{2}\alpha\overline{u}_1\overline{u}_{1x} - \tfrac{1}{2}\epsilon\rho_r\mathscr{T}_c[\overline{u}_{1xt}] + \alpha\epsilon\rho_r\left(\tfrac{11}{16}\mathscr{T}_c[\overline{u}_1^2]_{xx} - \tfrac{1}{4}\overline{u}_{1x}\mathscr{T}_c[\overline{u}_{1x}] - \tfrac{3}{8}\overline{u}_1\mathscr{T}_c[\overline{u}_{1xx}]\right) = 0, \tag{A 19}$$

where $\rho_r = \rho_2/\rho_1$ and the error terms are $O(\epsilon^2, \alpha^3, \alpha^2\epsilon)$. Likewise, the equation for ζ can be written as

$$\zeta_t + \zeta_x - \tfrac{3}{2}\alpha\zeta\zeta_x + \tfrac{1}{2}\epsilon\rho_r\mathscr{T}_c[\zeta_{xx}] - \tfrac{3}{8}\alpha^2\zeta^2\zeta_x - \alpha\epsilon\rho_r\left(\tfrac{9}{16}\mathscr{T}_c[\zeta^2]_{xx} + \tfrac{1}{2}\zeta_x\mathscr{T}_c[\zeta_x] + \tfrac{5}{8}\zeta\mathscr{T}_c[\zeta_{xx}]\right) = 0. \tag{A 20}$$

Once again, when we assume the balance between nonlinear and dispersive effects $\alpha = O(\epsilon)$, the following higher-order linear dispersive term of $O(\epsilon^2)$ (Matsuno 1994)

$$-\tfrac{3}{8}\epsilon^2\left(\rho_r^2 - \tfrac{4}{9}\right)\zeta_{xxx} \tag{A 21}$$

needs to be added to (A 20). By taking $\epsilon = \alpha = 1$, all physical variables in (A 19)–(A 20) can be regarded as being non-dimensionalized with respect to h_1 and c_0. The dimensional form of (A 20) can be written as

$$\frac{1}{c_0}\zeta_t + \zeta_x - \frac{3}{2h_1}\zeta\zeta_x + \frac{\rho_r h_1}{2}\mathscr{T}_c[\zeta_{xx}] - \frac{3}{8h_1^2}\zeta^2\zeta_x - \rho_r\left(\tfrac{9}{16}\mathscr{T}_c[\zeta^2]_{xx} + \tfrac{1}{2}\zeta_x\mathscr{T}_c[\zeta_x] + \tfrac{5}{8}\zeta\mathscr{T}_c[\zeta_{xx}]\right) = 0. \tag{A 22}$$

As in the case of the shallow water configuration, both (A 19) and (A 20) conserve a mass-like integral such as $\int_{-\infty}^{+\infty}\overline{u}_1\,\mathrm{d}x$ or $\int_{-\infty}^{+\infty}\zeta\,\mathrm{d}x$ for (A 19) and (A 20), respectively, but these equations do not seem to possess a conservation law that contains the energy-like variable $\overline{u}_1^2$ or ζ^2. We can correct this by using the leading-order equation from the first three terms in (A 19) in the form

$$\mathscr{T}_c[\overline{u}_{1xt}] + \mathscr{T}_c[\overline{u}_{1xx}] + \tfrac{3}{4}\alpha\mathscr{T}_c[\overline{u}_1^2]_{xx} = O(\epsilon), \tag{A 23}$$

and adding it to (A 19) multiplied by the factor $-\frac{5}{4}\epsilon\rho_r$. In this way we obtain the equation

$$\overline{u}_{1t} + \overline{u}_{1x} + \tfrac{3}{2}\alpha\overline{u}_1\overline{u}_{1x} - \tfrac{7}{4}\epsilon\rho_r\mathscr{T}_c[\overline{u}_{1xt}] - \tfrac{5}{4}\epsilon\rho_r\mathscr{T}_c[\overline{u}_{1xx}] - \tfrac{1}{8}\alpha\epsilon\rho_r\left(2\mathscr{T}_c[\overline{u}_1^2]_{xx} + 2\overline{u}_{1x}\mathscr{T}_c[\overline{u}_{1x}] + 3\overline{u}_1\mathscr{T}_c[\overline{u}_{1xx}]\right) = 0, \tag{A 24}$$

which conserves the definite sign integral

$$\mathscr{E} = \frac{1}{2}\int_{-\infty}^{+\infty}\left(\overline{u}_1^2 - \frac{7\epsilon\rho_r}{4}\overline{u}_1\mathscr{T}_c[\overline{u}_{1x}]\right)\mathrm{d}x, \tag{A 25}$$

as one can check easily. Similarly, one can find from (A 20) an equation for ζ possessing an energy conservation law,

$$\zeta_t + \zeta_x - \tfrac{3}{2}\alpha\zeta\zeta_x - \tfrac{1}{4}\epsilon\rho_r\mathscr{T}_c[\zeta_{xt}] + \tfrac{1}{4}\epsilon\rho_r\mathscr{T}_c[\zeta_{xx}] \\ -\tfrac{3}{8}\alpha^2\zeta^2\zeta_x - \alpha\epsilon\rho_r\left(\tfrac{3}{8}\mathscr{T}_c[\zeta^2]_{xx} + \tfrac{1}{2}\zeta_x\mathscr{T}_c[\zeta_x] + \tfrac{5}{8}\zeta\mathscr{T}_c[\zeta_{xx}]\right) = 0. \quad \text{(A 26)}$$

It is easy to verify that the flow governed by this equation conserves the integral

$$\mathscr{E} = \frac{1}{2}\int_{-\infty}^{+\infty}\left(\zeta^2 - \frac{\epsilon\rho_r}{4}\zeta\mathscr{T}_c[\zeta_x]\right)\,\mathrm{d}x. \quad \text{(A 27)}$$

REFERENCES

Abramowitz, M. & Stegun, I. A. 1970 *Handbook of Mathematical Functions*. Dover.

Benjamin, T. B. 1966 Internal waves of finite amplitude and permanent form. *J. Fluid Mech.* **25**, 241–270.

Benjamin, T. B. 1967 Internal waves of permanent form of great depth. *J. Fluid Mech.* **29**, 559–592.

Byrd, P. F. & Friedman, M. D. 1954 *Handbook of Elliptic Integrals for Engineers and Physicists*. Springer.

Camassa, R., Holm, D. D. & Levermore, C. D. 1996 Long-time effects of bottom topography in shallow water. *Physica* D **98**, 258–286.

Camassa, R. & Levermore, C. D. 1997 Layer-mean quantities, local conservation laws, and vorticity, *Phys. Rev. Lett.* **78**, 650–653.

Choi, W. & Camassa, R. 1996*a* Weakly nonlinear internal waves in a two-fluid system. *J. Fluid Mech.* **313**, 83–103.

Choi, W. & Camassa, R. 1996*b* Long internal waves of finite amplitude. *Phys. Rev. Lett.* **77**, 1759–1762.

Davis, R. E. & Acrivos, A. 1967 Solitary internal waves in deep water. *J. Fluid Mech.* **29**, 593–607.

Evans, W. A. B. & Ford, M. J. 1996 An integral equation approach to internal (2-layer) solitary waves. *Phys. Fluids* **8**, 2032–2047.

Fletcher, C. A. J. 1990 *Computational Techniques for Fluid Dynamics*, *Volume I*: *Fundamental and General Techniques*. Springer.

Funakoshi, M. & Oikawa, M. 1986 Long internal waves of large amplitude in a two-layer fluid. *J. Phys. Soc. Japan* **55**, 128–144.

Gradshteyn, I. S. & Ryzhik, I. M. 1994 *Tables of Integrals, Series, and Products*, 5th Edn. Academic.

Green, A. E. & Naghdi, P. M. 1976 A derivation of equations for wave propagation in water of variable depth. *J. Fluid Mech.* **78**, 237–246.

Grue, J., Friis, H. A., Palm, E. & Rusas, P. O. 1997 A method for computing unsteady fully nonlinear interfacial waves. *J. Fluid Mech.* **351**, 223–252.

Joseph, R. I. 1977 Solitary waves in finite depth fluid. *J. Phys.* A: *Math. Gen.* **10**, L225–L227.

Koop, C. G. & Butler, G. 1981 An investigation of internal solitary waves in a two-fluid system. *J. Fluid Mech.* **112**, 225–251.

Kubota, T., Ko, D. R. S. & Dobbs, L. D. 1978 Propagation of weakly nonlinear internal waves in a stratified fluid of finite depth. *AIAA J. Hydrodyn.* **12**, 157–165.

Laget, O. & Dias, F. 1997 Numerical computation of capillary-gravity interfacial solitary waves. *J. Fluid Mech.* **349**, 221–251.

Lamb, H. 1932 *Hydrodynamics*. Dover.

Liska, R., Margolin, L. & Wendroff, B. 1995 Nonhydrostatic two-layer models of incompressible flow. *Computers Math. Applics.* **29**, 25–37.

Matsuno, Y. 1993 A unified theory of nonlinear wave propagation in two-layer fluid systems. *J. Phys. Soc. Japan* **62**, 1902–1916.

Matsuno, Y. 1994 Phase shift of interacting algebraic solitary waves in a two-layer fluid system. *Phys. Rev. Lett.* **73**, 1316–1319.

Miyata, M. 1985 An internal solitary wave of large amplitude. *La Mer* **23**, 43–48.

Ono, H. 1975 Algebraic solitary waves in stratified fluids. *J. Phys. Soc. Japan* **39**, 1082–1091.
Segur, H. & Hammack, J. L. 1982 Soliton models of long internal waves. *J. Fluid Mech.* **118**, 285–304.
Tung, K., Chan, T. F. & Kubota, T. 1982 Large amplitude internal waves of permanent form. *Stud. Appl. Maths* **66**, 1–44.
Whitham, G. B. 1974 *Linear and Nonlinear Waves*. Wiley.
Wu, T. Y. 1981 Long waves in ocean and coastal waters. *J. Engng Mech. Div. ASCE* **107**, 501–522.